scientific reports

Check for updates

OPEN

Optimized FOPID controller for steam condenser system in power plants using the sinh-cosh optimizer

Serdar Ekinci[1], Davut Izci[2,3], Veysel Gider[4], Laith Abualigah[5,6], Mohit Bajaj[7,8,9]✉ & Ievgen Zaitsev[10,11]✉

Steam condensers in power plants are crucial for improving the efficiency of the power generation cycle by condensing and recycling steam from the turbine. We used fractional-order proportional-integral-derivative (FOPID) controller to regulate the pressure inside the steam condenser system. We adopted sinh-cosh optimizer (SCHO) to tune this controller. We analyzed the pressure fluctuations and transient responses to verify the system balance between different operational states. Several well-known algorithms, including the gravitational search algorithm, whale optimization algorithm, manta ray foraging optimization and aquila optimizer, are tested against the SCHO. The simulation demonstrates that the SCHO-based method outperforms other approaches in terms of integral of time-weighted absolute error (ITAE), normalized overshoot, and normalized settling time. The SCHO-based FOPID controller attained a minimal error of 14.80 for ITAE, a minimum percentage overshoot of 6.06%, and the shortest settling time of 17.66 s. The stated values confirm that SCHO-based FOPID controller offers superior and more consistent performance for the system under study. Nonlinear analyses further demonstrate the efficacy of the proposed method in terms of circulating water outlet temperature, cooling water flow rate, steam heat and condenser pressure.

Keywords Steam condenser, FOPID controller, Sinh-Cosh optimizer, Energy, Nonlinear control

In modern industrial uses, heat exchangers, particularly steam condensers, have very significant contributions to the efficiency and reliability of power plant and chemical process. The main idea behind the steam condensers is to make power generation efficient by condensing the exhaust steam from turbines, hence making it possible to reuse condensed water. However, these systems are extremely difficult to control because of nonlinear dynamics, along with the need for high precision regulation of temperature and pressure.

Most widely used controllers for steam condensers are proportional-integral-derivative (PID) controllers. Traditional PID controllers have been widely used in industrial control systems due to their simplicity and ease of implementation. While effective in many applications, PID controllers can struggle with highly non-linear or complex systems, as their limited tuning flexibility often results in suboptimal performance. To overcome this, the fractional-order PID (FOPID) controller is developed. FOPID controllers introduce two additional parameters, λ (the fractional order of the integrator) and (the fractional order of the differentiator). This increased flexibility allows FOPID controllers to fine-tune the system response more precisely, especially in systems with complex dynamics, such as steam condensers. The ability to adjust the fractional orders of the

[1]Department of Computer Engineering, Batman University, Batman 72100, Turkey. [2]Department of Electrical and Electronics Engineering, Bursa Uludag University, Bursa 16059, Turkey. [3]Applied Science Research Center, Applied Science Private University, Amman 11931, Jordan. [4]Distance Education Application and Researcher Center, Batman University, Batman, Turkey. [5]Computer Science Department, Al al-Bayt University, Mafraq 25113, Jordan. [6]Centre for Research Impact & Outcome, Chitkara University Institute of Engineering and Technology, Chitkara University, Rajpura, Punjab 140401, India. [7]Department of Electrical Engineering, Graphic Era (Deemed to be University), Dehradun 248002, India. [8]College of Engineering, University of Business and Technology, Jeddah 21448, Saudi Arabia. [9]Graphic Era Hill University, Dehradun 248002, India. [10]Department of Theoretical Electrical Engineering and Diagnostics of Electrical Equipment, Institute of Electrodynamics, National Academy of Sciences of Ukraine, Beresteyskiy, 56, Kyiv-57, Kyiv 03680, Ukraine. [11]Center for Information-Analytical and Technical Support of Nuclear Power Facilities Monitoring, National Academy of Sciences of Ukraine, Akademika Palladina Avenue, 34-A, Kyiv, Ukraine. ✉email: thebestbajaj@gmail.com; zaitsev@i.ua

integral and derivative terms enables better handling of transient responses and steady-state errors, leading to improved control accuracy and stability[1–5]. However, the complexity of system dynamics and the increased number of parameters make the tuning of the FOPID controller challenging.

Various optimization strategies have been suggested by researchers to tackle these problems. In this regard, metaheuristic algorithms have become very popular because they are capable of finding optimum solutions within complex search spaces, without using gradient information, since they emulate natural processes. Several optimization techniques are reported in the literature regarding the control of steam condensers and other similar industrial processes. For example, Rashedi et al.[6] introduced the gravitational search algorithm (GSA) to optimize these systems, with very good results being reached. The whale optimization algorithm (WOA) by Mirjalili and Lewis[7] has been proven to be effective for handling systems that are dynamic and nonlinear. The manta ray foraging optimization (MRFO) technique proposed by Zhao et al.[8] is one such example that has already shown outstanding efficiency in engineering applications. The aquila optimizer (AO) implemented by Abualigah et al.[9] has successfully reached effective results in different kinds of industrial applications.

In the rapidly evolving field of renewable energy systems, effective control strategies are critical for maintaining stability and optimizing performance. The integration of intermittent sources such as solar and wind energy has introduced challenges that require sophisticated controllers, such as PID and FOPID, to manage power quality and ensure grid stability. Recent advancements in optimization techniques and intelligent controllers have demonstrated significant improvements in these areas. Researchers are increasingly focusing on the application of hybrid optimization algorithms and fractional-order controllers to enhance the robustness and adaptability of power systems. Ekinci et al.[10] proposed a novel hybrid educational competition optimizer, combined with pattern search and a cascaded PDN-PI controller, which showed significant improvement in frequency regulation of PV-reheat thermal power systems. This approach addresses dynamic challenges commonly faced in renewable energy systems by balancing robustness and precision, an important factor in modern control applications. Building upon this, Jabari et al.[11] extended the application of optimization techniques to DC motor speed control using a multi-stage FOPD(1 + PI) controller. Their work highlights the importance of adaptive control, especially in dynamic systems, showcasing the Pelican optimization algorithm's effectiveness in achieving higher precision and faster response times, which are crucial for maintaining system stability. Goud et al.[12] contributed to power quality enhancement by introducing a GSA-FOPID controller in PV-integrated systems. Their study focuses on mitigating power quality issues such as harmonics and voltage fluctuations, critical aspects in renewable energy systems where variability in input can challenge grid stability. Goud et al.[13] further advanced this by addressing voltage sag and swell through a Black Widow optimization-based FOPID controller, a significant step in maintaining voltage stability in renewable networks. Kalyan et al.[14] introduced the Squirrel Search Algorithm-based intelligent controller, which was applied to interconnected power systems. This approach underlined the need for scalable control strategies to manage distributed power systems, aligning with the growing complexity of modern energy grids. The intelligent controllers demonstrated significant improvements in handling power distribution across diverse renewable energy sources. In line with these advancements, Gopi et al.[15] proposed the V-Tiger PID controller for automatic voltage regulation, ensuring robustness and stability under varying operational conditions. This development highlights the importance of robust control in renewable energy applications, where fluctuating inputs require sophisticated adaptive control mechanisms to ensure grid reliability. Kalyan et al.[16] explored frequency regulation in geothermal power plants, utilizing a 3DOFPID controller in a multi-source system. Their approach provides insights into how controllers can be optimized for different renewable sources, making the control more flexible across various energy types. Similarly, Goud et al.[17] focused on improving power quality using distributed power flow controllers with a Black Widow optimization-based FOPID controller, further emphasizing the role of hybrid optimization techniques in managing distributed energy systems. Kalyan et al.[18] and Goud et al.[19] also explored the effectiveness of Water Cycle Algorithms in optimizing 3DOF-PID controllers in multi-area power systems. These studies demonstrate the critical need for advanced optimization techniques to handle the complexities of multi-source energy grids, ensuring stability under fluctuating load conditions. Prasad et al.[20] addressed power management in hybrid AC-DC microgrids through an ANFIS PID controller optimized using the Elephant Herding Optimization algorithm. Their work underscores the importance of adaptive fuzzy logic controllers in managing the hybrid nature of modern power systems, providing essential insights into how intelligent controllers can optimize energy efficiency and stability in real-world scenarios.

In terms of steam condensers, several attempts were reported[21–30] to improve the performance of the system. These studies have examined diverse control methodologies targeted at improving the dynamic response, lifetime, and controllability of steam condensers. Chen et al.[31] evaluated and improved the thermal performance of a steam power plant using dynamic modeling, simulation, and optimization strategies. The research carried out dynamic simulations to develop and verify a model of a crucial subcentral power plant with the inclusion of reheating and regeneration cycles. Thereafter, they analyzed the control of the plant as regards its ability to withstand sudden coal load changes. Maidi et al.[32] sought to enhance the control performance of a heat exchanger with an optimization approach on a linear proportional-integral controller. It was able to solve an unbounded optimization problem using a large-scale finite-dimensional model. Simulations showed very clearly the performance improvement of the controller over the others. Dugdale and Wen[33] have further enhanced the controls of the ammonia/steam exchanger by enhancing their PID controllers. They used three sets of PID controllers, which are used for ammonia temperature, pressure, and steam pressure. Using mathematical models and simulation techniques that adopt dynamic separation and strategy, the system successfully reached the target state without causing any problems. Wu and his team[34] address the standard pitfalls for the PID-based control system through an extensive description of arrangement, structure, and applied methods of control in fossil-fuel steam plants. Shin and his coworkers[35] developed a new method, based on temperature gradients, for assessing the thermal performance of steam condensers. The method can predict the pressure transition temperature.

Alzakari et al.[30] explored the application of a FOPID controller for the efficient control of a steam condenser. They used an enhanced cooperation search algorithm for tuning the FOPID controller. Through comparative testing, the proposed approach outperformed competitive algorithms, reducing overshoot by 55%, improving settling time by 11%, and enhancing system stability.

In light of the above discussion, this study applies a new metaheuristic algorithm known as the sinh-cosh optimizer (SCHO)[36] for optimizing the parameters of an FOPID controller in a steam condenser system. The SCHO was chosen for optimizing the FOPID controller due to its distinct approach to balancing exploration and exploitation. By utilizing the sinh and cosh functions, SCHO efficiently explores the search space while refining solutions through focused exploitation. This capability is critical when dealing with the non-linear and dynamic nature of the steam condenser system. Compared to other well-known algorithms SCHO demonstrates faster convergence, superior stability, and enhanced accuracy in achieving optimal control settings. These advantages make it a suitable candidate for this complex control problem. A performance evaluation of the proposed method was performed by comparing it with several other widely recognized optimization methods such as GSA, WOA, MRFO, and AO. The FOPID controller, optimized using the SCHO, achieved impressive performance metrics, including an integrated time absolute error value as low as 14.80, a minimal percentage overshoot of 6.06%, and the fastest settling time recorded at 17.66 s. These performance indicators clearly demonstrate the effectiveness and reliability of the SCHO-based FOPID controller in regulating the system under consideration. Additionally, nonlinear analysis further highlights the robustness of this approach. Key parameters such as the circulating water outlet temperature, cooling water flow rate, steam heat, and condenser pressure were all efficiently controlled, showcasing the controller's capability to handle complex system dynamics and maintain optimal operational conditions. This consistent performance across various critical parameters underscores the superiority of the SCHO-based FOPID controller compared to alternative control methods.

Sinh-Cosh optimizer

The SCHO is a metaheuristic optimization approach that was inspired by the sinh and cosh functions, which are natural mathematical functions[36]. The SCHO successfully achieves optimal solutions in the search field by maintaining a balance between exploration and exploitation stages. Initially, an ensemble of N arbitrarily generated solutions (agents) is mounted. A candidate is represented by using each solution, which is distributed randomly in a D-dimensional space and evaluated by means of a particular fitness cost. The SCHO utilizes the sinh and cosh functions to effectively handle both exploration and exploitation phases, facilitating extensive search coverage and meticulous analysis. Equations (1) and (2) respectively describe the position update in SCHO where f_1 and f_2 depict the cosh and sinh mechanisms, respectively.

$$X_{(i,j)}^{t+1} = X_{(i,j)}^{t} + f_1\,(cosh) \tag{1}$$

$$X_{(i,j)}^{t+1} = X_{(i,j)}^{t} + f_2\,(sinh) \tag{2}$$

The sinh and cosh functions, which are essential components of the SCHO algorithm, provide diverse search strategies inside the solution space. The sinh function (hyperbolic sine) and cosh (hyperbolic cosine) are given by Eq. (3), (4).

$$sinh\,(x) = \frac{e^{x} - e^{-x}}{2} \tag{3}$$

$$cosh\,(x) = \frac{e^{x} + e^{-x}}{2} \tag{4}$$

Initialization

Similar to other metaheuristic algorithms, SCHO starts by means of randomly initializing a set of candidate answers. The initialization is represented as:

$$X = \begin{bmatrix} X_{1,1} & \cdots & X_{1,j} & X_{1,\dim-1} & \cdots & X_{1,\dim} \\ X_{1,2} & \cdots & X_{2},j & \cdots & \cdots & X_{2,\dim} \\ \cdots & \cdots & X_{i,j} & \cdots & \cdots & \cdots \\ \vdots & \vdots & \vdots & \vdots & \vdots & \vdots \\ X_{N-1,1} & \cdots & X_{N-1,j} & \cdots & \cdots & X_{N-1,\dim} \\ X_{N,1} & \cdots & X_{N,j} & X_{N,\dim-1} & \cdots & X_{N,\dim} \end{bmatrix} \tag{5}$$

where is a set of random candidate solutions obtained via using Eq. (6), $X_{i,j}$ denotes the h position of h solution, represents the number of candidate solutions, and is the problem dimension. The initial positions are calculated as:

$$X = rand\ (N, dim)\ \times\ (ub - lb) + lb \tag{6}$$

where $rand$ is a random value in the range [0,1], and ub and lb represent the upper and lower bounds of the variables.

Exploration phase

In the exploration phase, the positions of search retailers are up to date based at the contemporary satisfactory solutions. Exploration is split into levels, with the transition fee defined as:

$$T = floor\left(\frac{t_{max}}{ct}\right) \tag{7}$$

where t_{max} is the maximum number of iterations, $floor$ rounds down to the nearest integer, and ct is a coefficient set to 3.6 in this study. The position update function for the first exploration phase is:

$$X_{(i,j)}^{t+1} = \begin{cases} X_{best}^{(j)} + r_1 \times W_1 \times X_{(i,j)}^{t}, & r_2 > 0.5 \\ X_{best}^{(j)} - r_1 \times W_1 \times X_{(i,j)}^{t}, & r_2 < 0.5 \end{cases} \tag{8}$$

where t indicates the current iteration, $X_{(i,j)}^{t}$ and $X_{(i,j)}^{t+1}$ mean the j-th position of the i-th solution in the current iteration and next iteration, respectively. $X_{best}^{(j)}$ is the j-th position of the optimal solution obtained so far, $r1/r2$ are the random numbers in the interval [0,1]. W_1 is the weight coefficient of $X_{(i,j)}^{t}$ in the first exploration phase, controlling candidate solutions in the first phase to stay away from themselves and gradually exploring towards the optimal solution, which is calculated using Eq. (9):

$$W_1 = r_3 \times a_1 \times (coshr_4 + u \times sinhr_4 - 1) \tag{9}$$

where a_1 is a monotonically decreasing function calculated as:

$$a_1 = 3 \times \left(-1.3 \times \frac{t}{t_{max}} + m\right) \tag{10}$$

with m being a precision coefficient controlling the accuracy of the exploration, set to 0.45 based on experiments. For the second exploration phase, the position update function is:

$$X_{(i,j)}^{t+1} = \begin{cases} X_{(i,j)}^{t} + |\epsilon \times W_2 \times X_{best}^{(j)} - X_{(i,j)}^{t}|, & r_5 > 0.5 \\ X_{(i,j)}^{t} - |\epsilon \times W_2 \times X_{best}^{(j)} - X_{(i,j)}^{t}|, & r_5 < 0.5 \end{cases} \tag{11}$$

where ϵ epsilon is a small positive number set to 0.003, and W_2 is calculated as:

$$W_2 = r_6 \times a_2 \tag{12}$$

with a_2 being another monotonically decreasing function calculated as:

$$a_2 = 2 \times \left(-\frac{t}{t_{max}} + n\right) \tag{13}$$

where n is a precision coefficient for the second exploration phase set to 0.5.

Exploitation phase

The exploitation phase ensures that candidate solutions concentrate around the optimal regions. For the first exploitation phase, the position update function is:

$$X_{(i,j)}^{t+1} = \begin{cases} X_{best}^{(j)} + r_7 \times W_3 \times X_{(i,j)}^{t}, & r_8 > 0.5 \\ X_{best}^{(j)} - r_7 \times W_3 \times X_{(i,j)}^{t}, & r_8 < 0.5 \end{cases} \tag{14}$$

where W_3 is calculated as:

$$W_3 = r_9 \times a_1 \times (coshr_{10} + u \times sinhr_{10}) \tag{15}$$

For the second exploitation phase, the position update function is:

$$X_{(i,j)}^{t+1} = X_{(i,j)}^{t} + r_{11} \times \frac{sinhr_{12}}{coshr_{12}} |W_2 \times X_{best}^{(j)} - X_{(i,j)}^{t}| \tag{16}$$

where W_2 is the precision coefficient in the second exploitation phase.

Constrained search strategy

The SCHO algorithm utilizes a restricted search technique to thoroughly investigate the whole possible search space. This approach entails conducting a comprehensive initial investigation, followed by a thorough inspection in successive iterations, which is systematically quantified as:

$$BS_{k+1} = BS_k + floor(\frac{t_{max} - BS_k)}{\alpha} \tag{17}$$

Let k be a positive integer, BS_k represents the current and next limited search iteration, and α is a coefficient set to 4.6.

$$BS_1 = floor(\frac{t_{max})}{\beta} \tag{18}$$

where β controls the starting value of the constrained search strategy, set to 1.55. The upper and lower bounds of the potential search space are calculated as:

$$ub_k = X_{best}^{(j)} + \left(1 - \frac{t}{t_{max}}\right) \times \left| X_{best}^{(j)} - X_{second}^{(j)} \right| \tag{19}$$

$$lb_k = X_{best}^{(j)} - \left(1 - \frac{t}{t_{max}}\right) \times \left| X_{best}^{(j)} - X_{second}^{(j)} \right| \tag{20}$$

The limits of the potential search space are determined by calculating the upper and lower bounds. The variables ub_k and lb_k denote the upper and lower bounds of the potential search space, $X_{second}(j)$. The symbol (j) denotes the $j-th$ location of the suboptimal solution.

Switching mechanism

The SCHO method employs a switching mechanism that utilizes the sinh and cosh functions to alternate between exploration and exploitation phases. This technique prioritizes exploration at some stage in the preliminary iterations and transitions to exploitation in next iterations. Exploration refers to the act of looking for new possibilities and amassing facts, at the same time as exploitation entails maximizing the benefits from the recognized possibilities.

$$A = \left[p - q \times \left(\frac{t}{t_{max}}\right)^{\frac{\cosh\frac{t}{t_{max}}}{\sinh\frac{t}{t_{max}}}} \right] \times r_{13} \tag{21}$$

Let r_{13} be a random number between 0 and 1. p and q are equilibrium coefficients which are equal to 10 and 9, respectively. The SCHO algorithm engages in exploration when the value of A is greater than 1, and in exploitation when the value of A is less than 1.

Figure 1 provides an overview of the four primary stages of the SCHO algorithm: exploration and exploitation phases, limited search method, and switching mechanism. Every step is meticulously crafted to enhance the

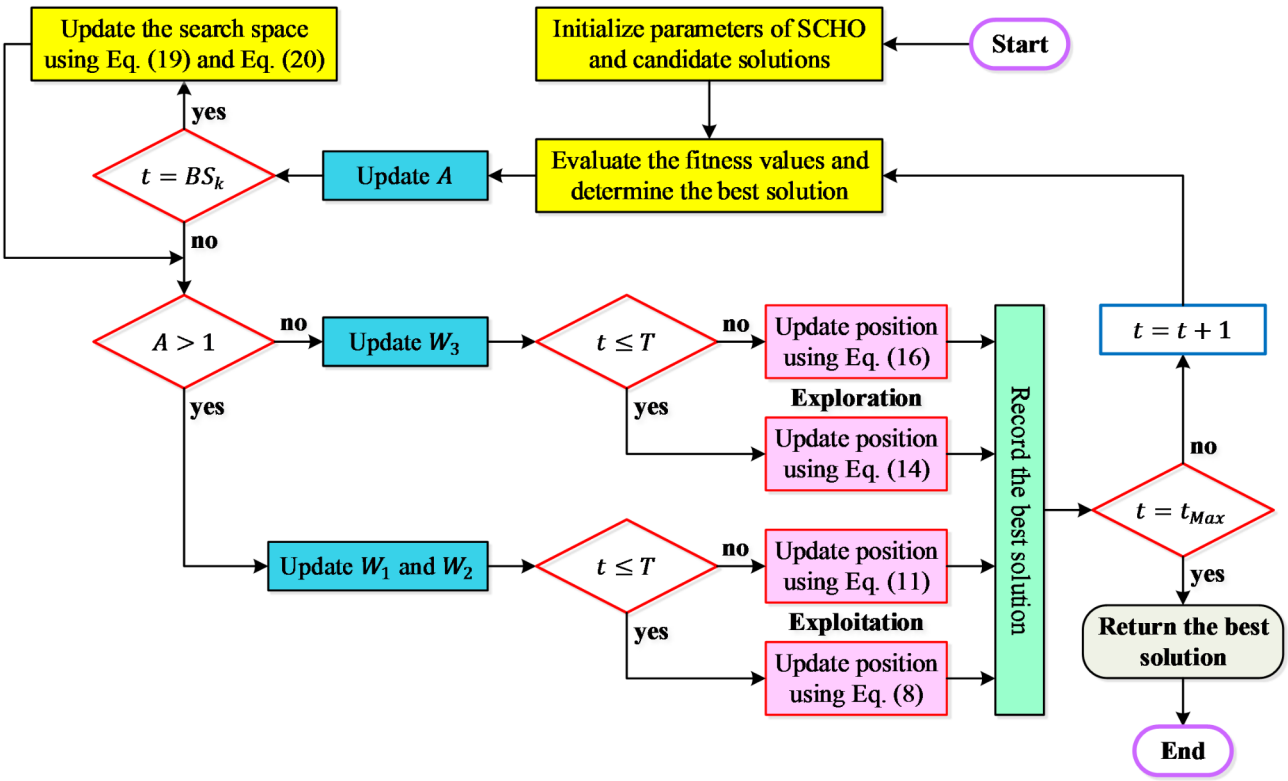


Fig. 1. Flowchart of SCHO.

algorithm's efficiency. The exploration phase involves surveying a broad region of the search space, while the exploitation phase concentrates on identifying the optimal solutions for more accurate and targeted searches. The constrained search method reduces the scope of the search to expedite the process, while the switching mechanism handles the shifts between these stages.

Dynamic modeling of a steam condenser

Power plants depend on a steam condenser to efficiently convert steam from the turbine into water for later use. Steam condensers require sophisticated control techniques to achieve optimal performance due to the intricate heat and mass transfer processes involved in their dynamic modeling[37–39]. Figure 2 depicts the fundamental configuration of the steam condenser, showcasing all the steam movements.

The mathematical model of the steam condenser system is based on several key assumptions to ensure its applicability and simplicity. These assumptions include steady-state operation, ideal gas behavior, negligible heat losses and simplified dynamic interactions. The model assumes that the system operates under steady-state conditions, minimizing the impact of transient effects. Besides, the steam and air inside the condenser are modeled as ideal gases, which simplifies the calculation of their thermodynamic properties. Moreover, the heat losses to the environment are considered negligible due to the use of insulation. Lastly, the interactions between the steam, air, and water flow are assumed to be linear and stable, ensuring consistent system performance. These assumptions provide a basis for the model's reliability and simplify the process of optimizing the FOPID controller.

Mathematical model of shell side of condenser

Steam zone

(i) Steam Mass Equation:

$$\frac{dG_s}{dt} = G_{st} + G_{ost} - G_c - G_{ss} \tag{22}$$

Equation (22) represents the mass balance of steam in the condenser. It states that the rate of change of steam mass $\frac{dG_s}{dt}$ in the condenser is equal to the steam entering from the steam turbine G_{st} and other steam inlets G_{ost}, minus the steam that condenses G_c and the steam drawn out by vacuum equipment G_{ss}. The unit of all parameters in this equation is kg/s. The mass balance equation for steam in the condenser (Eq. 22) governs the flow of steam entering from the turbine, steam that condenses, and the air removed by vacuum equipment. The total mass of steam inside the condenser is modeled as the sum of these components.

(ii) Steam Pressure Equation:

$$\frac{dP_s}{dt} = \frac{R_s\left(\frac{dG_s}{dt}\right)}{V}\ (T_s + 273.15) \tag{23}$$

Equation (23) describes the relationship between the steam pressure inside the condenser and the rate of change of steam mass. P_s is the internal steam pressure (Pa), R_s is the steam gas constant (0.4615 kJ/(kgK)), V is the volume of gas in the condenser (m^3), and T_s is the temperature of the saturated gas (°C).

(iii) Average Enthalpy of Steam:

$$\frac{d\left(G_s\, H_s\right)}{dt} = G_{st} \times H_{st} + G_{ost} \times H_{ost} - \left(G_c + G_{ss}\right) \times H_s \tag{24}$$

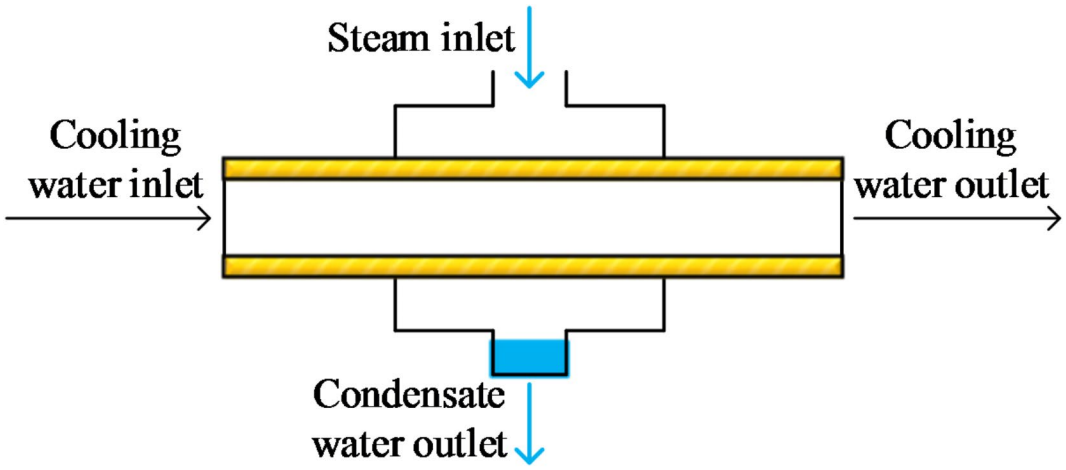


Fig. 2. Structure of a typical steam condenser.

Equation (24) expresses the change in total enthalpy of the steam in the condenser. It accounts for the enthalpy of the steam entering from the steam turbine and other inlets, minus the enthalpy of the condensed steam and the steam removed by vacuum equipment. Here, the average enthalpy of steam is H_s (kJ/kg), enthalpy of steam turbine exhaust is H_{st} (kJ/kg), enthalpy of other inlet is H_{ost} (kJ/kg). The enthalpy equation (Eq. 24) models the heat exchange between the steam, the condenser, and the condensed water. The change in total enthalpy represents the energy absorbed by the system, which is critical for understanding the temperature changes during operation.

Air zone
(i) Air Mass Equation:

$$\frac{dG_a}{dt} = G_{vb} + G_n + G_g - G_a \tag{25}$$

Equation (25) represents the mass balance of air in the condenser. G_a is the air mass (kg/s), G_{vb} is the air entering from the vacuum break valve $(\mathrm{kg/s})$, G_n is the air from normal drain condenser (kg/s), and G_g is the air from seal leakage (kg/s).

(ii) Air Pressure Equation:

$$\frac{dP_a}{dt} = \frac{R_a\left(\frac{dG_a}{dt}\right)}{V}\ (T_s + 273.15) \tag{26}$$

Equation (26) describes the relationship between the air pressure inside the condenser and the rate of change of air mass. P_a is the air pressure (P_a), R_a is the gas constant for air air (0.287 kJ/(kgK)), V is the volume of gas in the condenser, and T_s is the temperature of the saturated gas.

(iii) Absolute Pressure of the Condenser:

$$P_c = P_s + P_a \tag{27}$$

Equation (27) simply states that the absolute pressure inside the condenser (P_c) is the sum of the steam pressure (P_s) and the air pressure (P_a).

Hot water area
(i) Hot Well Water Level Equation:

$$L_c = \frac{G_w}{\rho\, A_w} \tag{28}$$

Equation (28) calculates the water level (L_c (m)) in the hot well based on the water mass (G_w (kg/s)), the density of water (ρ (kg/m³)), and the cross-sectional area of the hot well ($A_w(m^2)$).

(ii) Hot Water Quality Equation:

$$\frac{dG_w}{dt} = G_c + G_{gp} - G_{wo} \tag{29}$$

Equation (29) represents the mass balance of hot well water, considering the water entering from condensation (G_c), bubbling oxygen exhaust (G_{gp}), and the water leaving the condenser (G_{wo}).

(iii) Enthalpy Equation of Hot Well Water:

$$\frac{d\,(G_w\,H_w)}{dt} = G_c{}^*\,H_{cw} + G_{gp}{}^*\,H_{gp} - G_{wo}{}^*\,H_w \tag{30}$$

Equation (30) describes the change in total enthalpy of the hot well water, taking into account the enthalpy of the condensed water, bubbling oxygen exhaust, and the water leaving the condenser. H_{gp}, bubbling oxygen exhaust steam enthalpy (kJ/kg), H_w , enthalpy of hot well water (kJ/kg), H_{cw}, enthalpy of saturated water corresponding to the condenser pressure (kJ/kg).

Mathematical model of condenser tube side

Dynamic heat balance equation of circulating water:

$$M_w C_w \frac{dT_2}{dt} = Q - Q_w = UA\Delta\, t_m - F_{cw}\, C_p\ (T - T_{cw}) \tag{31}$$

Equation (31) represents the dynamic heat balance of the circulating water in the condenser tubes. M_w is the mass of circulating water (kg), C_w is the heat capacity of water (kJ/(kg°C)), Q is the heat transferred from the steam to the water (kJ), Q_w is the heat absorbed by the water (kJ), U is the heat transfer coefficient (W/(m²°C)), A is the heat transfer area (m²), $\Delta\, t_m$ is the logarithmic mean temperature difference (°C), F_{cw} is the flow rate of the circulating water (kg/s), C_p is the specific heat capacity (kJ/(kg°C)), T is the outlet temperature (°C), and T_{cw} is the inlet temperature (°C).

Logarithmic heat transfer temperature difference:

$$\Delta t_m = \frac{(T - T_{cw})}{\ln\left[\frac{(T_s - T_{cw})}{T_s - T}\right]} \tag{32}$$

Equation (32) calculates the logarithmic mean temperature difference (Δt_m), which is a key parameter in determining the effectiveness of heat exchangers.

Overcooling of condenser is calculated by:

$$\Delta t_w = T_c - T_w \tag{33}$$

Equation (33) measures the overcooling (Δt_w) in the condenser by comparing the temperature of the condensed water (T_w) to the saturated water temperature corresponding to the vapor pressure (T_c).

Heat transfer error of the condenser is calculated by:

$$\delta_t = T_s - T \tag{34}$$

Equation (34) calculates the heat transfer error (δ_t) in the condenser by comparing the saturated gas temperature (T_s) with the outlet temperature (T).

The parameters in the condenser tube model were validated using a combination of experimental data and simulation results. Data from prior studies and real-world observations were used to ensure that the heat transfer coefficients, mass flow rates, and temperature differences reflected actual condenser behavior. Simulations were conducted using MATLAB/Simulink to replicate the dynamic behavior of the condenser tube system under different operating conditions. These simulations helped confirm the accuracy of the parameters. A sensitivity analysis was performed to evaluate how variations in parameters, such as the heat transfer coefficient and flow rate, impact the system's performance.

FOPID controller

FOPID controller is an extension of the classical PID controller, incorporating fractional orders for the integral and derivative terms. The control law of the FOPID controller is given by Eq. (35):

$$Con_{FOPID}(s) = K_P + \frac{K_I}{s^\lambda} + K_D s^\mu \tag{35}$$

Figure 3 shows the structure of the FOPID controller. The FOPID controller has fractional integral and derivative terms in addition to classical PID controllers. This structure provides more flexible and precise control.

Proposed design method

The proposed design method in this study involves optimizing the FOPID controller parameters using the SCHO algorithm. For steam condenser systems, the integral of time-weighted absolute error (ITAE) criterion is minimized to optimize the FOPID controller parameters. The ITAE criterion evaluates the system's performance and the controller's effectiveness.

The optimization problem and parameter constraints are shown in Eq. (36):

$$ITAE = \int_0^\infty t \cdot |e(t)| \cdot dt \tag{36}$$

where $e(t)$ is the error signal over time. Minimizing the ITAE ensures both small error and quick response time[40]. The ITAE criterion was selected as the primary performance metric for optimizing the FOPID controller

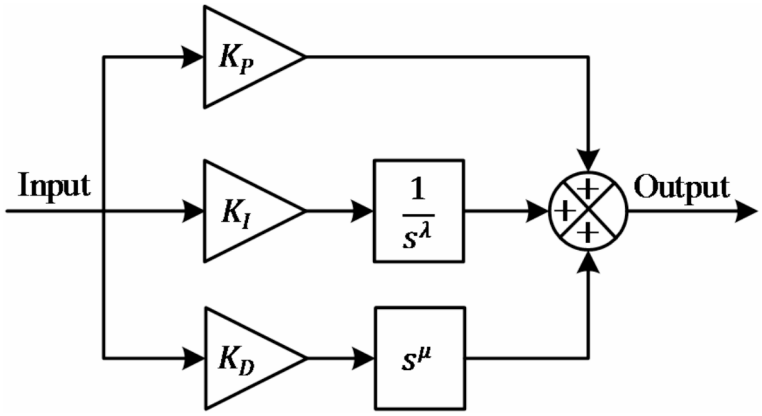


Fig. 3. Block diagram of FOPID controller.

because of its ability to penalize long-lasting errors more heavily. In contrast to other commonly used criteria such as IAE or ISE, which treat errors equally regardless of when they occur, ITAE emphasizes minimizing errors that persist over time. This makes it particularly effective in applications where long-term system stability is paramount, such as in steam condenser control, where sustained deviations can lead to inefficiencies or even system failures. ITAE was chosen because it promotes both a quick initial response and long-term error minimization, ensuring that the controller performs effectively over the entire operational range.

The parameter ranges for the FOPID were carefully selected based on research on FOPID controller and the system dynamics. FOPID controlled systems in similar non-linear processes as they provide a baseline for the parameter ranges, thus, allows us to ensure consistency with established methodologies. Besides, the steam condenser's non-linear dynamics required parameter ranges that would allow the controller to be robust under a variety of operating conditions, including changes in steam load and pressure. These considerations were essential for ensuring that the SCHO could effectively find the optimal parameter values for stable and efficient system performance. In light of these criteria, the limits set for the FOPID controller parameters are as $1 \leq K_P \leq 20,\ 0.1 \leq K_I \leq 10,\ 0.05 \leq K_D \leq 1,\ 0.5 \leq \lambda \leq 1.5$ and $0.5 \leq \mu \leq 1.5$.

Figure 4 shows the optimization process of FOPID controller parameters with the proposed SCHO algorithm. The optimization process includes steps to minimize the ITAE value. Figure 4 explains how the algorithm is applied and how the optimization process progresses. The implementations were carried out using MATLAB/Simulink on a Windows computer equipped with a 12th Gen Intel i5-12400, 2.50 GHz processor, and 16.00 GB RAM. The steps for the implementation of the SCHO, in Fig. 4, can be summarized as follows:

- Pressure setpoint: Apply the pressure setpoint to the condenser system.
- Error calculation: Calculate the difference between the setpoint and the output condenser pressure as an error.
- FOPID Controller: The error signal enters the FOPID controller. The controller uses a FOPID control strategy to generate an appropriate control signal.
- Updated parameters: Optimize the FOPID controller parameters ($K_P,\ K_I,\ K_D,\ \lambda,\ \mu$) using the SCHO algorithm.
- Nonlinear system: Apply this control signal to the steam condenser system and observe the condenser pressure.
- ITAE calculation: Calculate the ITAE based on the system response.
- SCHO optimization: Minimize the ITAE value and update the FOPID controller parameters to provide optimal control performance.

Simulation results

This section examines the efficacy of the SCHO in comparison to other widely used optimization algorithms from the literature, including GSA, WOA, MRFO, and AO. Table 1 presents a concise overview of the metrics and variables that are essential for accurately assessing the performance of a system. The table include both the

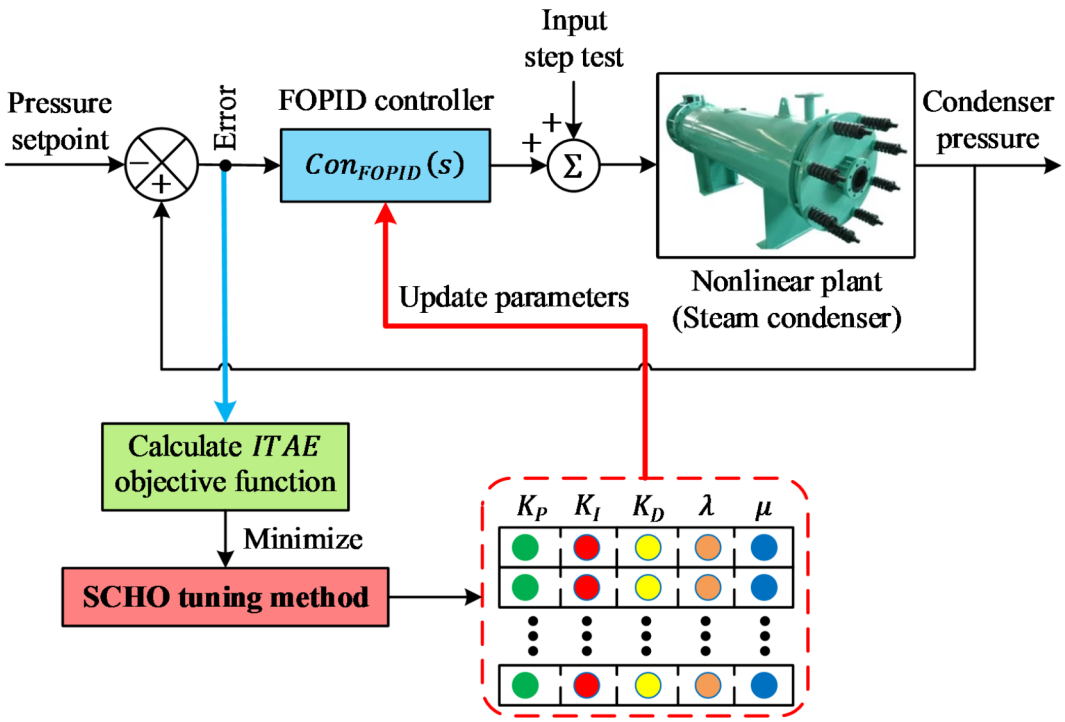


Fig. 4. SCHO-based optimization process for FOPID controlled steam condenser system.

Parameter/Variable	Value	Unit
R	0.461526	kJ/kgK
V	3	m^3
λ	2265.65	kJ/kg
UA	356.972	kW/K
M_{cw}	6500	kg
C_p	4.2	$kJ/\left(kgK\right)$
α	0.3162	K/kPa
β	68.0958	°C
α_1	0.087292	–
α_2	0.00073787	–
F_s	4	kg/s
F_c	4	kg/s
F_{cw}	107.8881	kg/s
P	90	kPa
T	80	°C
T_{cw}	60	°C
T_c	96.5538	°C
Q	9062.6	kW

Table 1. System parameters and variables[21].

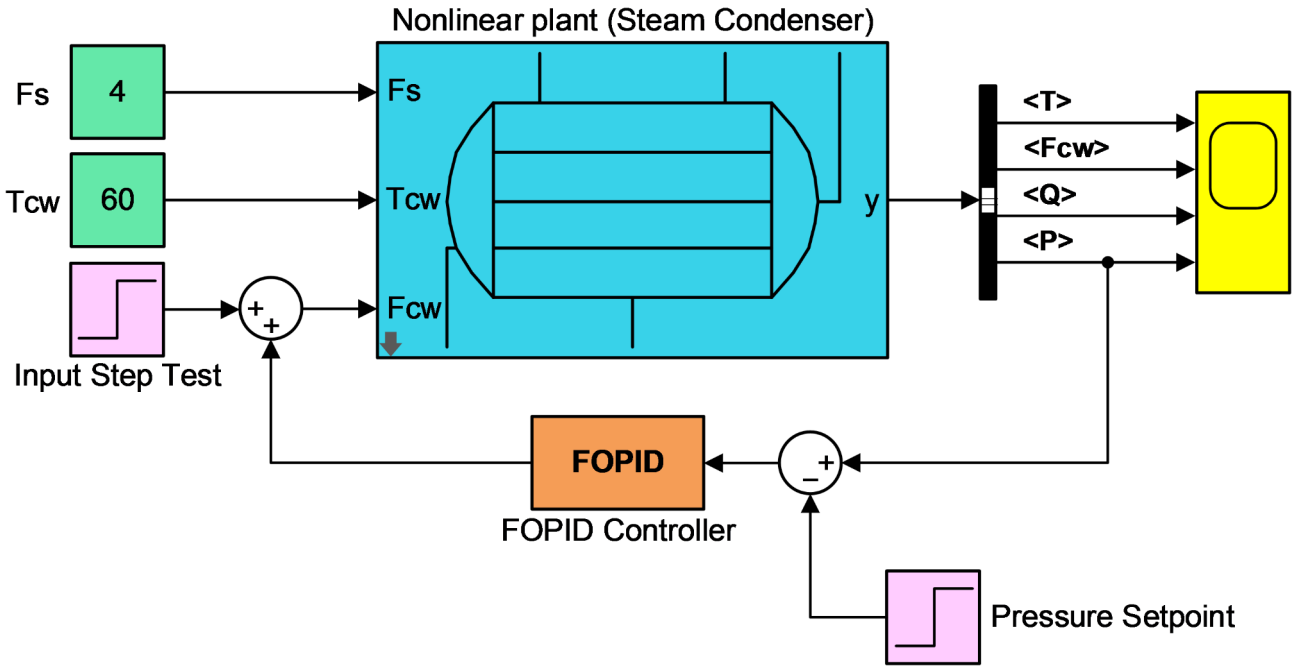


Fig. 5. Simulink-based dynamic modelling of a steam condenser with FOPID controller.

values and units for each parameter. Accurately comprehending these factors is crucial for the system to function efficiently and dependably.

Simulink model

Figure 5 depicts the dynamic modeling of a steam condenser using Simulink, incorporating the FOPID controller. The Simulink modeling replicates the dynamic behavior of the system and assesses the performance of the controller. The model comprises the inputs and outputs of the system, as well as the control loops and feedback mechanisms.

Algorithms	Population size	Total iteration number	Other control parameters
SCHO	30	40	$ct = 3.6,\ u = 0.388,\ m = 0.45, \varepsilon = 0.003,\ n = 0.5,\ \alpha = 4.6,\ \beta = 1.55,\ p = 10,\ q = 9$
GSA	30	40	$G_0 = 100,\ \alpha = 20$
WOA	30	40	$a = [0,\ 2],\ a_2 = [-2, -1],\ b = 1$
MRFO	30	40	$S = 2$
AO	30	40	$\alpha = 0.1,\ \delta = 0.1$

Table 2. Parameters of the algorithms.

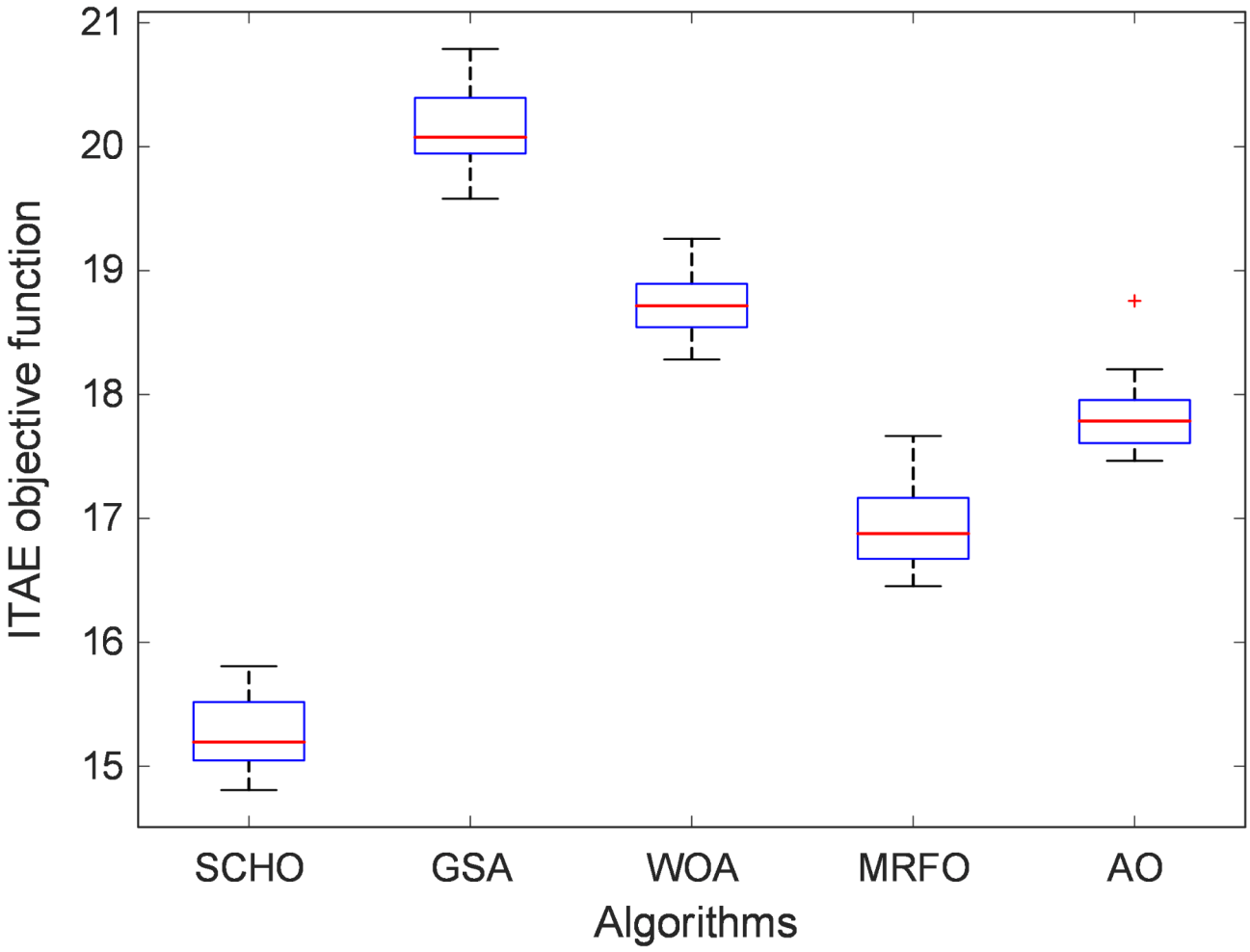


Fig. 6. Statistical boxplot analysis.

Compared algorithms

This section analyzes the parameters and performance of various optimization algorithms, such as GSA, WOA, MRFO, and AO, in comparison to the SCHO method. Table 2 presents numerical values of the control parameters utilized by each algorithm. The performance of the algorithms is directly influenced by the parameter values.

Statistical boxplot analysis

Figure 6 depicts a statistical boxplot study that compares the distribution of performance among several methods[41,42]. We employ statistical boxplot analysis to assess the performance distribution of several methods. The performance of each algorithm is assessed using statistical measures such as the median, interquartile, and end values. The examination of the boxplot indicates that the SCHO has the lowest variability in performance and demonstrates more stability compared to other algorithms. The reduced variability observed in the SCHO demonstrates its superior stability compared to the other algorithms. Lower variability in the optimization outcomes indicates that the SCHO consistently converges to near-optimal solutions, regardless of initial conditions or minor system disturbances. This reduced variability enhances the algorithm's stability, meaning that the SCHO-optimized FOPID controller is less likely to experience significant performance fluctuations

Algorithms	Minimum	Maximum	Average	Median	SD	Rank
SCHO	14.8078	15.8073	15.2538	15.1958	0.2733	1
GSA	19.5806	20.7887	20.1422	20.0760	0.2989	5
WOA	18.2824	19.2569	18.7342	18.7157	0.2758	4
MRFO	16.4532	17.6658	16.9018	16.8777	0.3234	2
AO	17.4650	18.7557	17.8288	17.7864	0.2866	3

Table 3. Statistical performance results of SCHO and other algorithms.

Metric	SCHO versus GSA	SCHO versus WOA	SCHO versus MRFO	SCHO versus AO
p-value	1.2290E – 05	1.2290E – 05	1.2290E – 05	1.2290E – 05
Winner	SCHO	SCHO	SCHO	SCHO

Table 4. Results of Wilcoxon signed-rank test.

when subjected to varying operational conditions. The consistency in control performance, as shown in the boxplots, highlights the robustness of the SCHO in producing reliable and stable outcomes, which is critical for maintaining control precision in dynamic industrial environments. The SCHO also yields dependable and uniform outcomes in parameter optimization. Based on the numerical data, the SCHO has a lower median ITAE of 15.1958 compared to the other algorithms. Additionally, it has a reduced interquartile range. Table 3 presents a comparison of the statistical performance of SCHO and other algorithms. The obtained values demonstrate the statistical superiority of the SCHO.

Wilcoxon test

Table 4 indicates the consequences of the Wilcoxon signed-rank test to assess the performance differences among the SCHO and other algorithms. The Wilcoxon test outcomes prove that the SCHO algorithm plays appreciably higher than different algorithms. This demonstrates that SCHO's overall performance isn't always random and gives a real benefit. The Wilcoxon signed rank look at conducted to evaluate the disparities in overall performance among the SCHO and alternative algorithms[43]. The Wilcoxon test findings display that the SCHO famous a statistically enormous superiority over different algorithms. This illustrates that the performance of SCHO is not arbitrary and gives a tangible advantage.

Convergence curve of objective function

Figure 7 shows the convergence curves of the objective function for various optimization techniques. The convergence curves show the value at which the algorithms converge to the optimal solution[44]. The SCHO method is famous for its improved convergence speed and stability compared to other algorithms.

Evolution of controller parameters

Figures 8, 9, 10, 11, 12 illustrate the change of the FOPID controller parameters (tuned with different algorithms) in detail with respect to iteration numbers. Figures 8, 9, 10, 11, 12 provide a detailed illustration of the change that occurs in the FOPID controller parameters (for various algorithms) based on the number of iterations. The best FOPID controller parameters obtained from 25 runs of the SCHO, GSA, WOA, MFO, and AO algorithms are listed in Table 5,

Nonlinear simulation results

Figure 13 illustrates the step change in the pressure setpoint of the system, where the pressure increases from 90 kPa to 95 kPa at approximately 10 s. This step input serves as a test signal to evaluate the controllers' ability to adapt to sudden changes in system conditions. A robust controller should respond quickly to this setpoint change while maintaining stability and minimizing overshoot. As observed in the transient response curves, the SCHO-optimized controller demonstrates the fastest adaptation to the new setpoint with minimal oscillations, highlighting its superior control performance.

Figure 14 presents the time-domain response of the circulating water outlet temperature for different algorithms under the same system conditions. At first glance, the curves may appear similar, but closer inspection reveals the distinct advantages of the SCHO-optimized controller. The SCHO approach exhibits the fastest settling time, achieving stability approximately at 17.66 s, compared to 20.08 s for GSA and marginally slower responses for other algorithms. The overshoot is also significantly reduced, preventing excessive fluctuations that could negatively impact system efficiency. These transient improvements are critical for minimizing energy consumption and ensuring the steady performance of the system, especially under sudden changes in operating conditions. Furthermore, the steady-state behavior confirms the SCHO controller's ability to maintain minimal deviation from the desired setpoint, underscoring its robust and precise regulation of the circulating water temperature.

Figure 15 depicts the time response of the cooling water flow across various algorithms. While the response trends may seem identical due to the system's inherent dynamics, a detailed analysis shows that the SCHO-

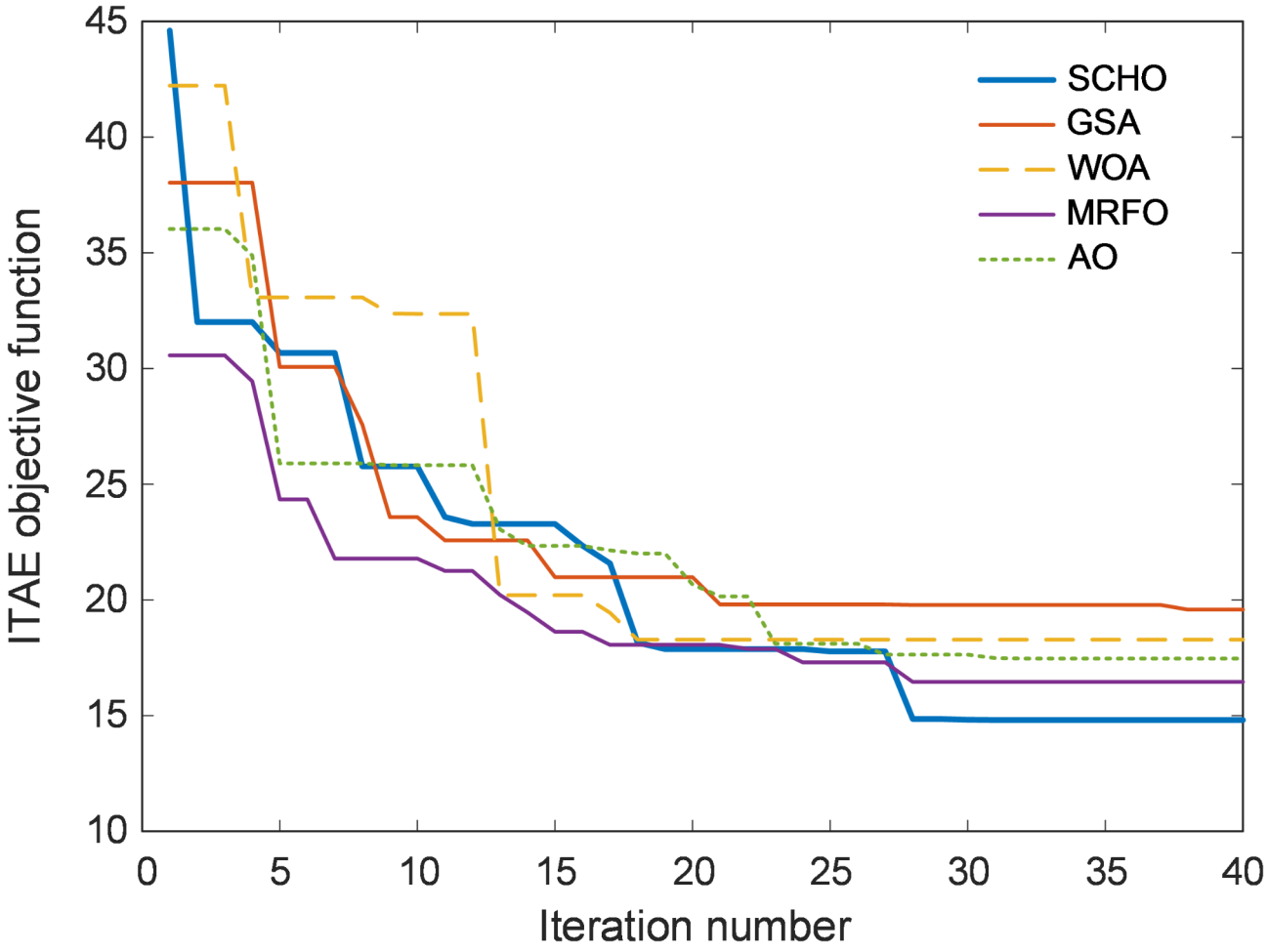


Fig. 7. Convergence curves of the ITAE objective function.

optimized controller stabilizes the flow faster and with greater robustness under dynamic conditions. This transient response improvement ensures consistent cooling water flow, which is critical for maintaining heat exchange efficiency and protecting the condenser system from thermal stress. Even under potential disturbances, the SCHO-based approach demonstrates resilience, reducing the likelihood of performance degradation or system instability.

Figure 16 focuses on the transient response of steam heat in the system. The SCHO-optimized controller exhibits faster stabilization, achieving a settling time of approximately 17.66 s compared to the slower convergence of other algorithms. Additionally, the overshoot in the steam heat response is minimized, which is crucial for maintaining efficient thermal energy transfer and avoiding unnecessary energy losses. By reducing transient oscillations and achieving a smoother response curve, the SCHO-based controller ensures improved operational stability and energy efficiency in real-world applications.

Figure 17 illustrates the time-domain response of condenser pressure, a critical parameter for maintaining the system's operational stability. The SCHO-optimized controller outperforms all other algorithms in terms of transient performance metrics, achieving the shortest settling time (17.66 s) and the lowest overshoot (6.06%). This performance advantage is crucial for regulating the condenser pressure effectively, especially during sudden operational changes. The reduced settling time and overshoot minimize the risks of system instability and mechanical stress, enhancing the overall reliability and longevity of the system. These results are particularly relevant for industrial applications where precise pressure control is critical for optimal performance.

The numerical data in Table 6 provides a quantitative comparison of the key time-domain performance metrics—ITAE, normalized overshoot, and settling time—for all algorithms. The SCHO consistently achieves the best results across all metrics: The SCHO controller attains the lowest value of **14.8078**, indicating superior overall transient performance by minimizing errors over time. The SCHO-based approach also achieves the smallest overshoot of **6.06%**, demonstrating its ability to avoid excessive fluctuations and maintain stable system behavior. With the shortest settling time of **17.66 s**, the SCHO algorithm ensures rapid stabilization of system parameters. These metrics collectively highlight the superiority of the SCHO-optimized FOPID controller, confirming its ability to deliver both transient and steady-state performance advantages over alternative optimization techniques. This combination of rapid adaptation and precise steady-state regulation ensures

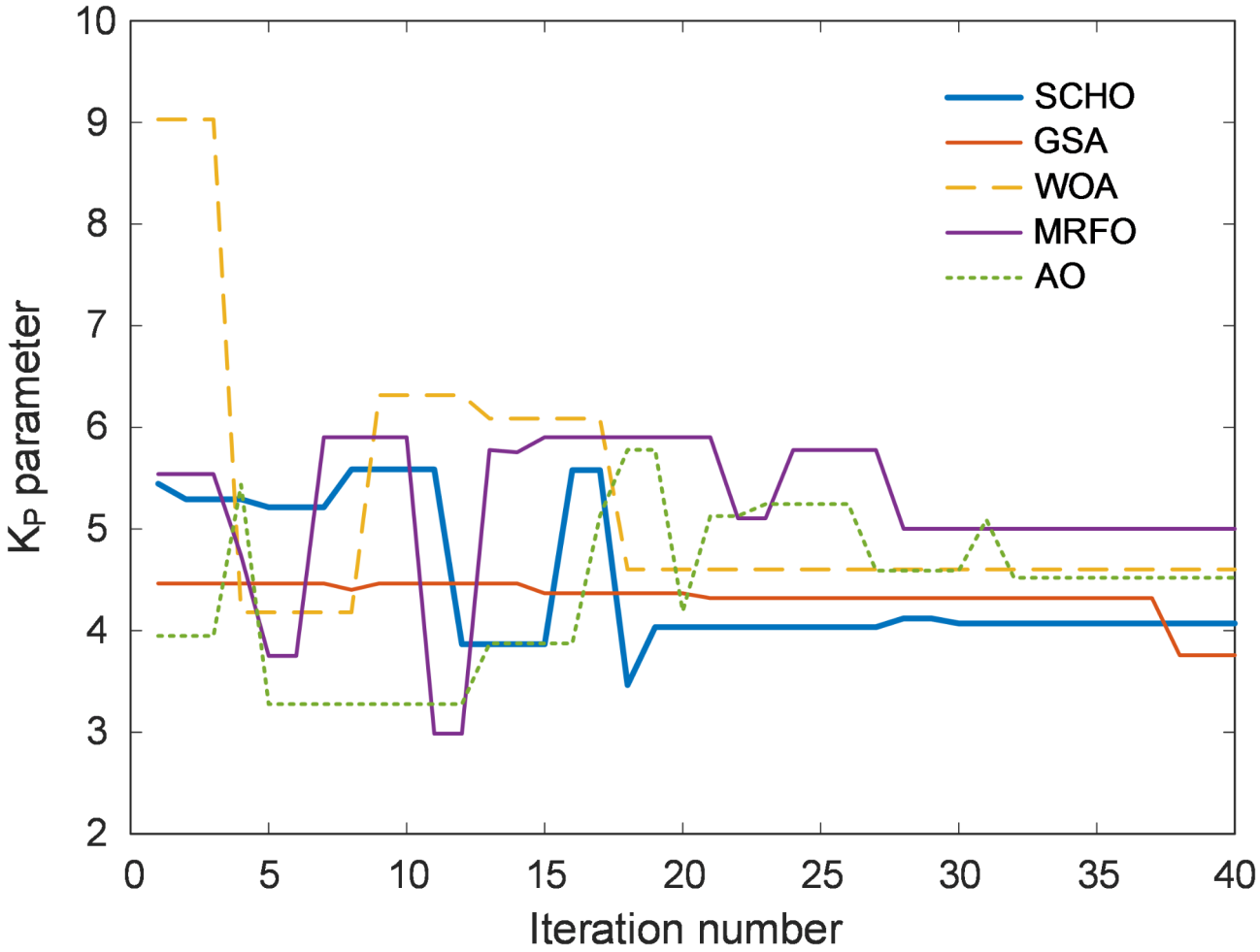


Fig. 8. Variation of K_P parameter

optimal system performance under dynamic conditions, making the SCHO-based approach a robust and efficient solution for steam condenser systems.

Impact of overcooling and heat transfer errors

This section explores the influence of overcooling and heat transfer errors on the overall system performance, particularly focusing on the steam condenser's energy efficiency and control stability. Our simulations, as presented in Section 6.7, highlight the importance of minimizing these errors for optimal system behavior.

Overcooling, which occurs when the temperature of the condensate drops below the necessary operational value, was observed to increase the system's energy consumption without improving condensation efficiency. By allowing the temperature to fall too low, the system requires additional energy to return to optimal operating conditions. This impact can be seen in the temporal variation of cooling water outlet temperature, as depicted in Fig. 14, where the SCHO algorithm minimizes these inefficiencies.

Similarly, heat transfer errors were found to cause temperature and pressure fluctuations, destabilizing the control system. Figure 17 presents the variations in condenser pressure, where the SCHO-optimized FOPID controller outperforms other algorithms by stabilizing the system more effectively. Minimizing these heat transfer errors is critical for maintaining system equilibrium and enhancing the overall performance of the steam condenser.

The ability of the SCHO algorithm to reduce overcooling and heat transfer errors is further evidenced by its superior performance metrics in Table 6, which compares the ITAE, normalized overshoot, and settling time of various algorithms. These results demonstrate that addressing these two factors—overcooling and heat transfer errors—significantly enhances system stability and efficiency.

Discussion

The FOPID controller, optimized using the SCHO, has been designed to adapt effectively to dynamic operating conditions, such as sudden load shifts and steam pressure changes. The fractional-order parameters allow for fine-tuning of the controller's behavior, providing greater flexibility in responding to system disturbances compared to traditional PID controllers. As demonstrated in Section 6.7, the FOPID controller maintained stable performance under varying conditions, with minimal impact on overshoot, settling time, and ITAE. This

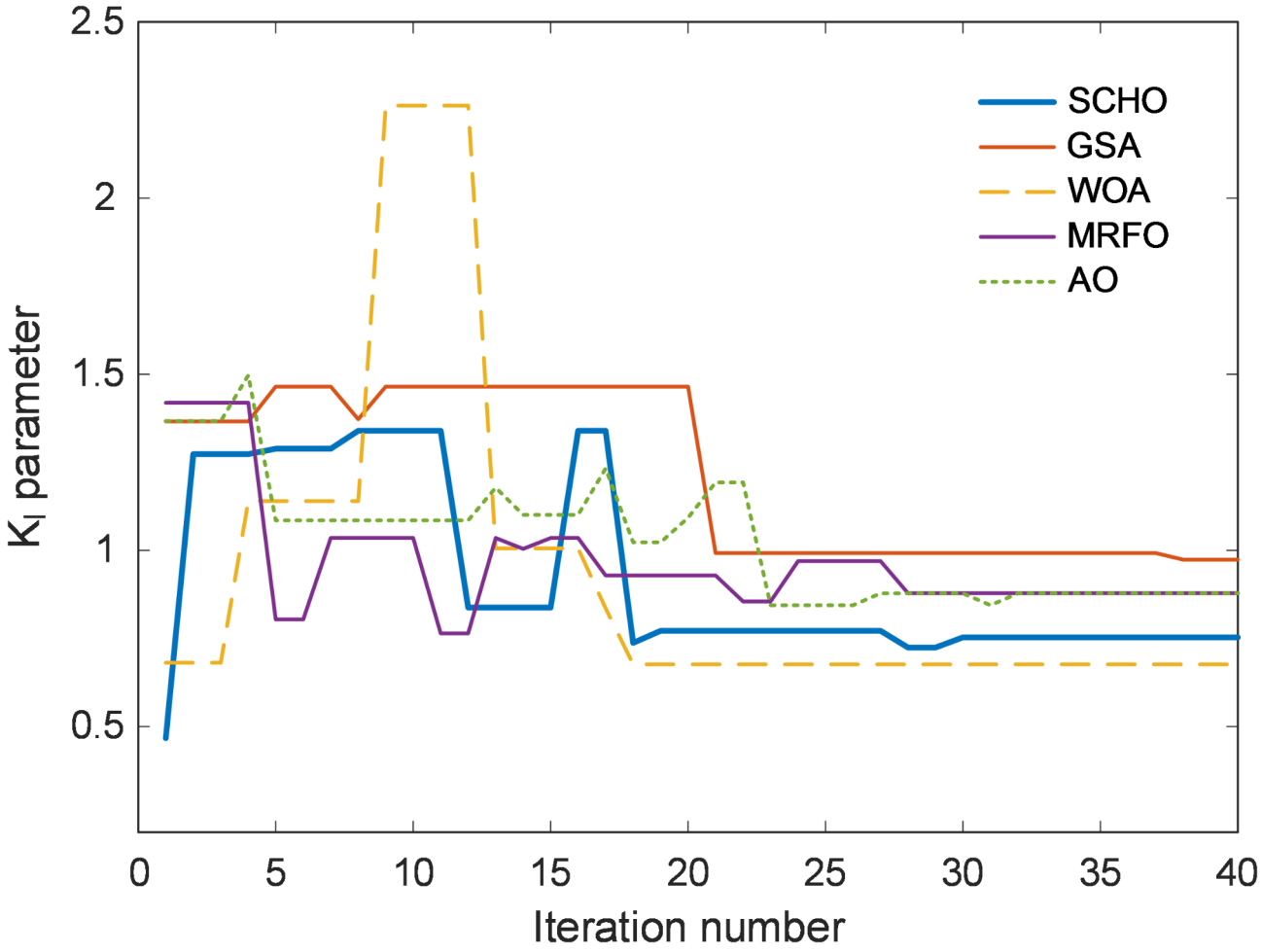


Fig. 9. Variation of K_I parameter

robustness ensures that the controller can handle real-world scenarios where sudden changes in system load or pressure are common, maintaining high control precision and stability. This adaptability makes the SCHO-optimized FOPID controller highly suitable for industrial applications where unpredictable operational changes occur.

While the SCHO has shown promising results in optimizing the FOPID controller for steam condenser systems, certain limitations must be acknowledged. In systems with high-dimensional search spaces or highly non-linear dynamics, the algorithm's convergence speed and accuracy may degrade, requiring additional iterations or more careful parameter tuning. Moreover, under extreme disturbance conditions, such as abrupt and large-scale fluctuations in system behavior, the performance of SCHO may be affected, potentially requiring additional robustness measures. These limitations suggest that further research could explore the development of hybrid optimization approaches that combine SCHO with other algorithms to enhance performance in complex control scenarios. Additionally, adaptive versions of the SCHO could be investigated to dynamically adjust its parameters based on real-time system feedback, ensuring sustained performance even under challenging conditions.

Conclusion

This work conducted a thorough analysis of the efficacy of the SCHO in optimizing the parameters of the FOPID controller in the steam condenser system. The results demonstrate that the SCHO outperforms other optimization algorithms in terms of its superior ITAE performance, high stability, dependability, and speedy convergence. The main benefit of the SCHO is its ability to minimize ITAE values in comparison to the other algorithms that were examined. The study successfully utilized the SCHO to improve the FOPID controller, resulting in a significant reduction in control error. The achieved ITAE value of 14.8078 represents the lowest recorded result. The ITAE values for the remaining algorithms are as follows: GSA (19.5806), WOA (18.2824), MRFO (16.4532), and AO (17.4650). SCHO has also attained the most minimal overshoot rate at 6.0647%, with GSA following at 10.6107%, WOA at 8.1506%, MRFO at 14.4882%, and AO at 12.4207%. Based on this data, it can be concluded that the SCHO algorithm offers more stability and consistency in terms of control performance. Upon optimization, it was shown that the SCHO algorithm exhibits the shortest settling time of

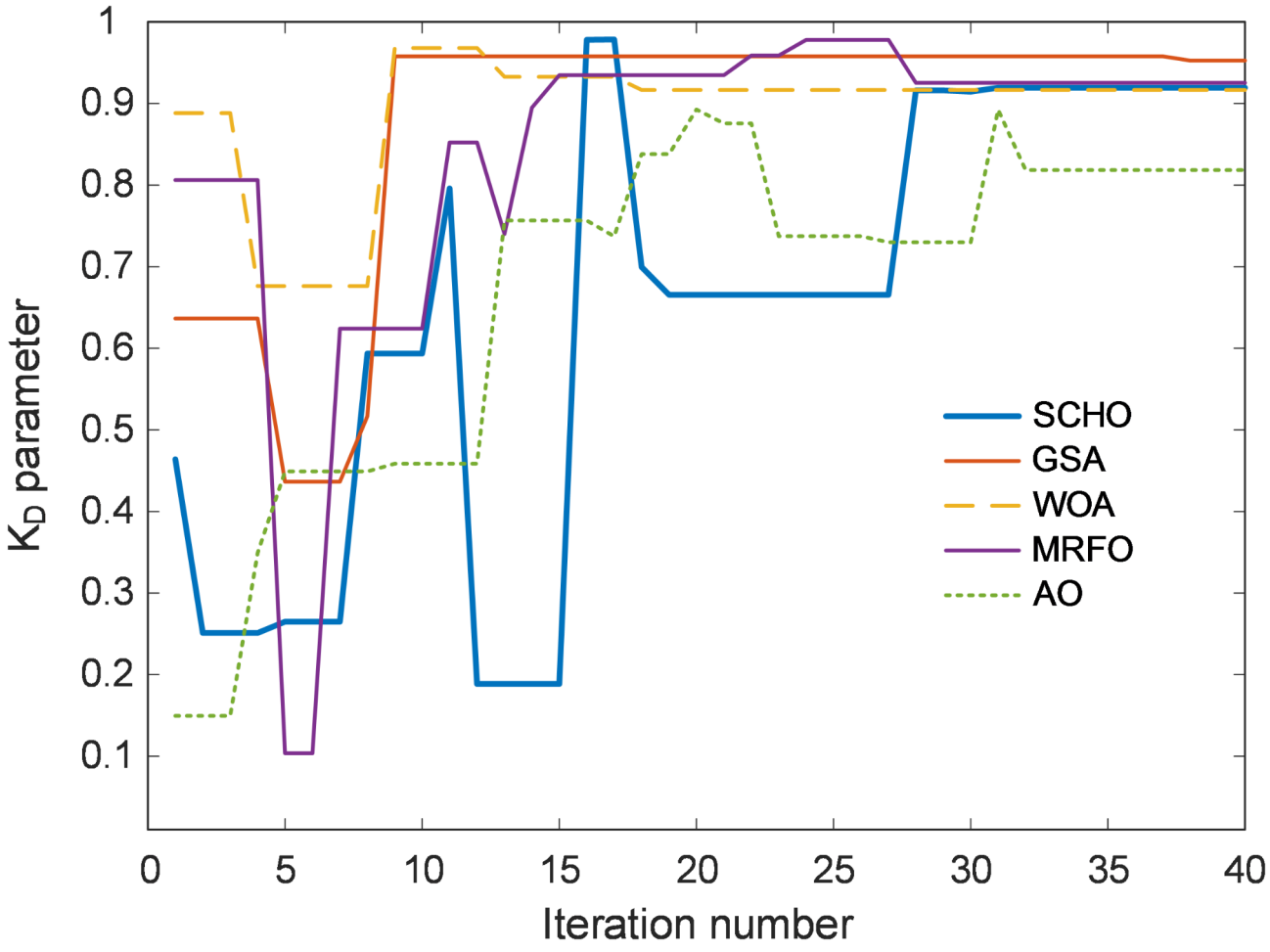


Fig. 10. Variation of K_D parameter

17.6635 s, hence offering superior stability in comparison to other methods. The GSA algorithm took 20.0770 s, the WOA algorithm took 17.9283 s, the MRFO algorithm took 17.0708 s, and the AO algorithm took 17.2855 s. The data shown above demonstrates that the SCHO algorithm consistently converges at a higher rate and exhibits more efficiency while operating with dynamic systems. Statistical analysis also revealed the low variability in performance and high stability of the SCHO algorithm.

The findings of this study have significant practical applications in the field of industrial control, particularly for steam condenser systems in power plants and other thermal processes. The optimized FOPID controller, tuned using the SCHO, can be implemented in real-world systems to improve energy efficiency by minimizing overcooling and optimizing heat transfer processes, which leads to reduced operational costs. It can also be used to enhance system stability by ensuring precise control of temperature and pressure within the steam condenser, resulting in fewer fluctuations and more consistent performance. It can help reducing wear and tear on mechanical components due to smoother system operation, potentially extending the lifespan of equipment. By integrating the optimized controller, industries can achieve greater control accuracy and better energy management[45–48], which is essential for both environmental sustainability and cost efficiency in large-scale operations. While the current study demonstrates the effectiveness of the SCHO-optimized FOPID controller, several areas of future research remain. Future work can extend the use of the SCHO to optimize controllers in other industrial settings, such as HVAC systems, refrigeration units, and chemical process plants, where similar benefits in energy efficiency and system stability could be realized. Moreover, combining the SCHO with other metaheuristic optimization techniques, such as GA or PSO, could lead to even more robust optimization solutions, especially for highly complex and dynamic systems.

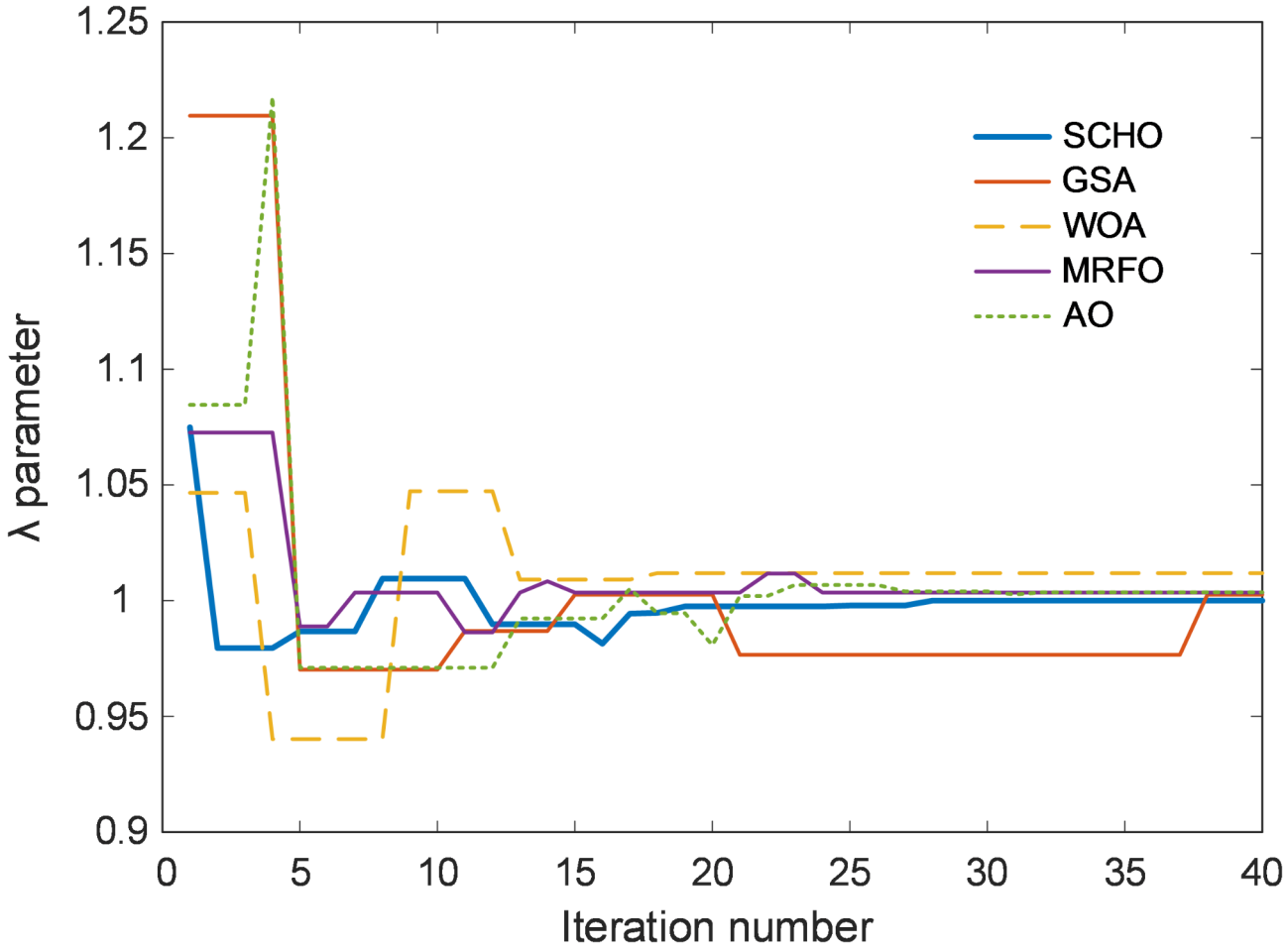


Fig. 11. Variation of λ parameter

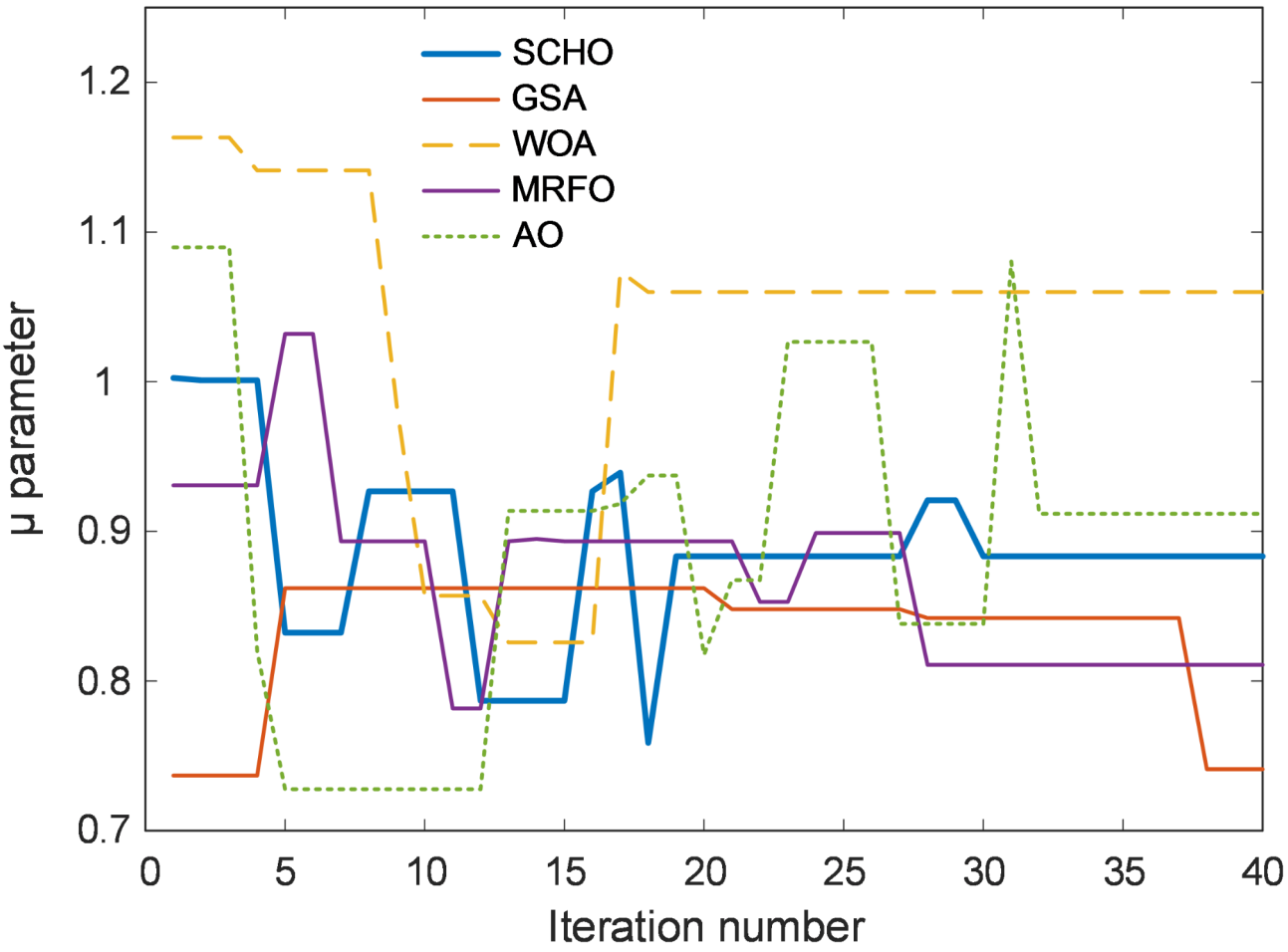


Fig. 12. Variation of μ parameter

Algorithms	K_P	K_I	K_D	λ	μ
SCHO	4.0709	0.7530	0.9194	1.0000	0.8833
GSA	3.7584	0.9740	0.9527	1.0026	0.7411
WOA	4.6027	0.6766	0.9167	1.0119	1.0599
MRFO	5.0016	0.8785	0.9253	1.0035	0.8108
AO	4.5205	0.8781	0.8185	1.0036	0.9118

Table 5. Best FOPID controller parameter optimized by various algorithms.

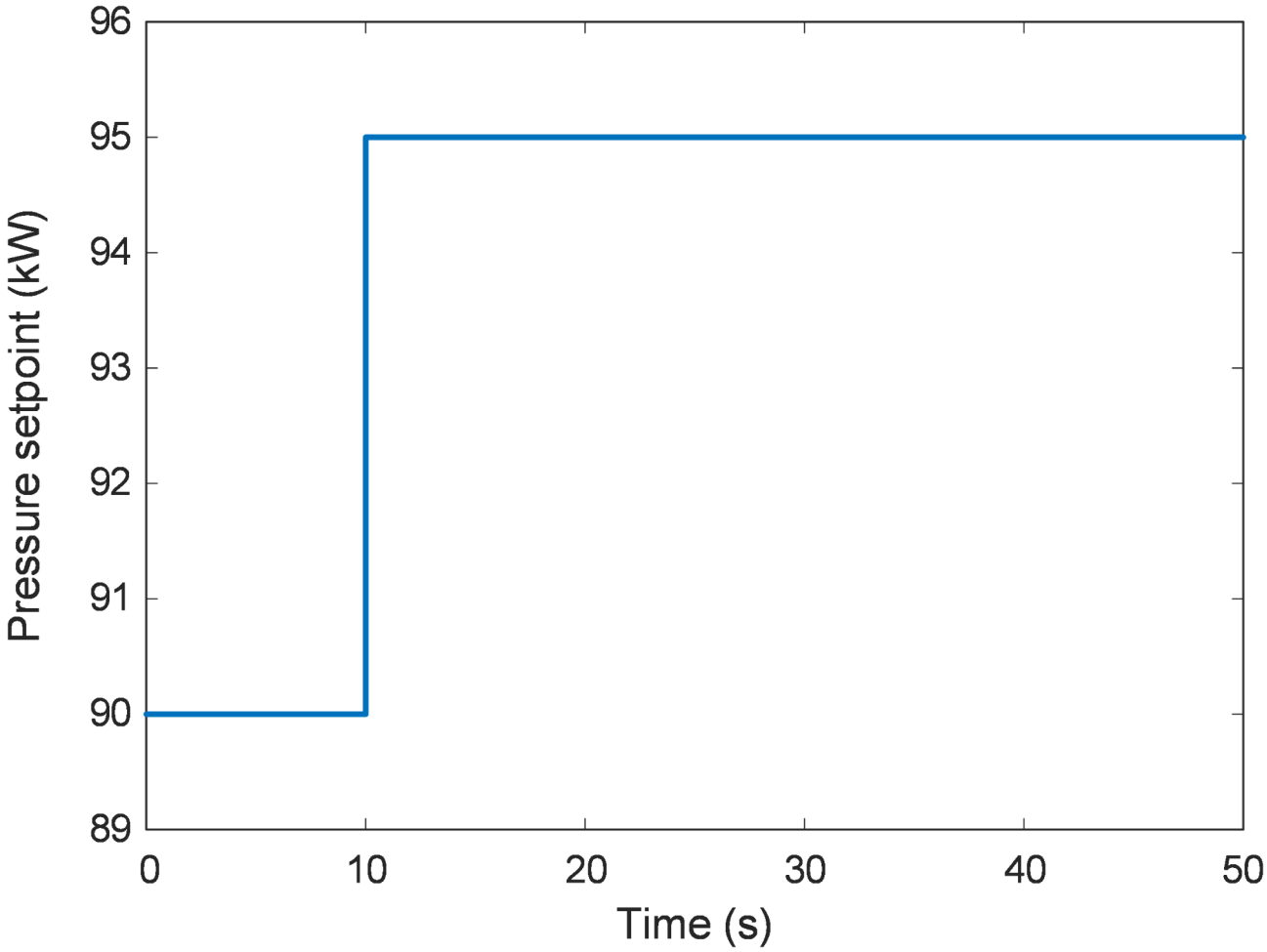


Fig. 13. Change of pressure setpoint (step change in P setpoint from 90 kPa to 95 kPa).

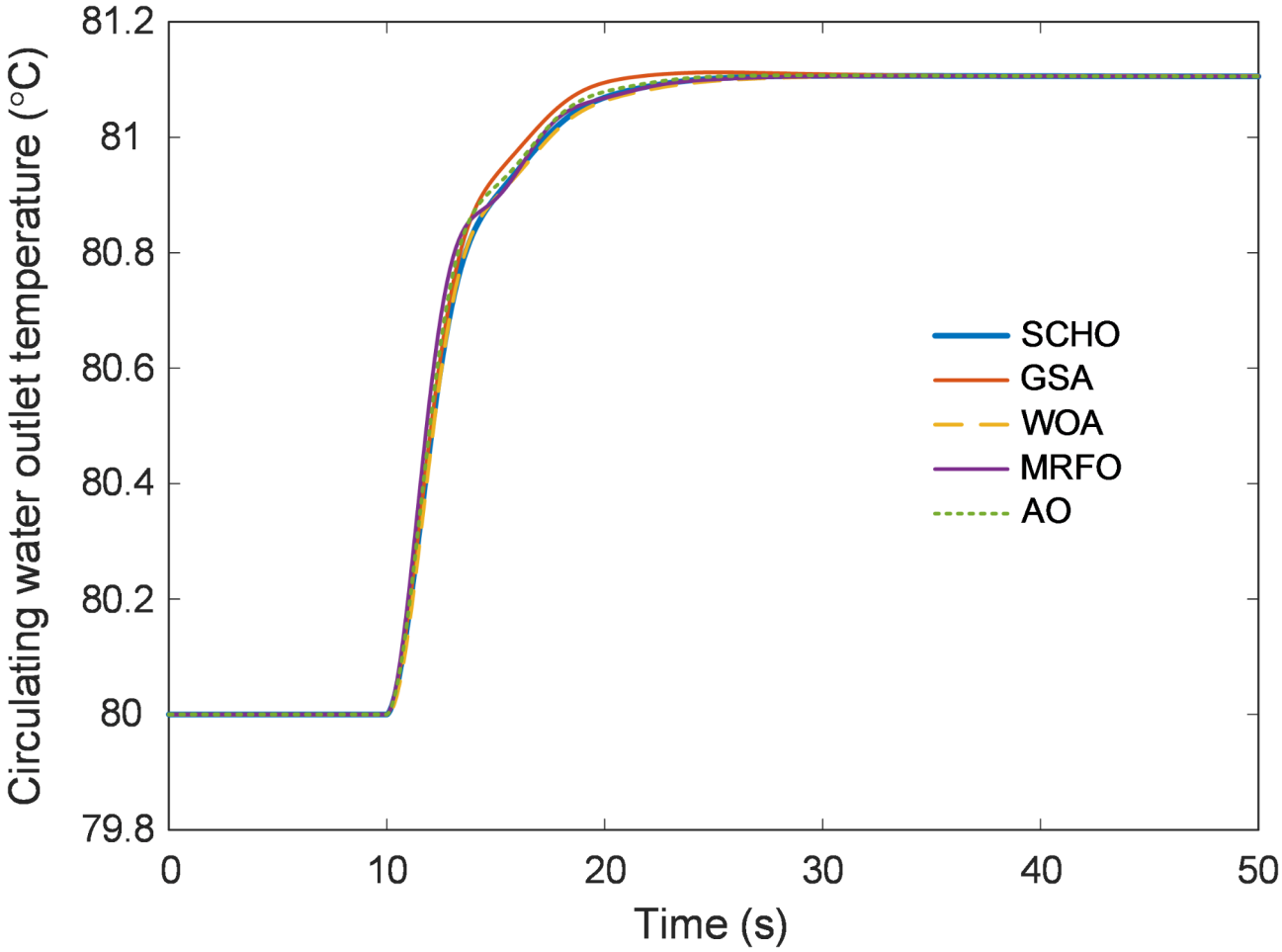


Fig. 14. Time response of circulating water outlet temperature.

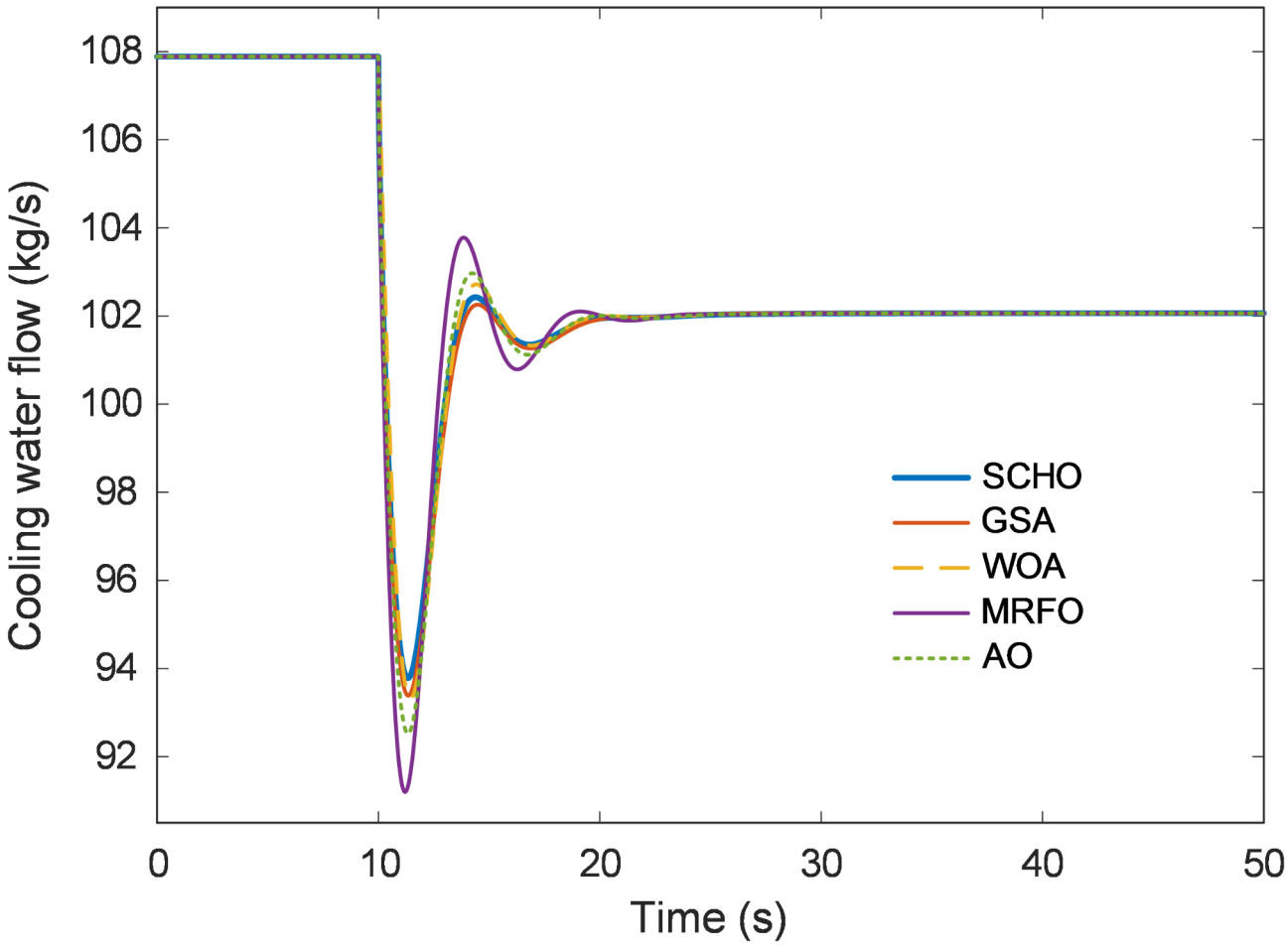


Fig. 15. Time response of cooling water flow.

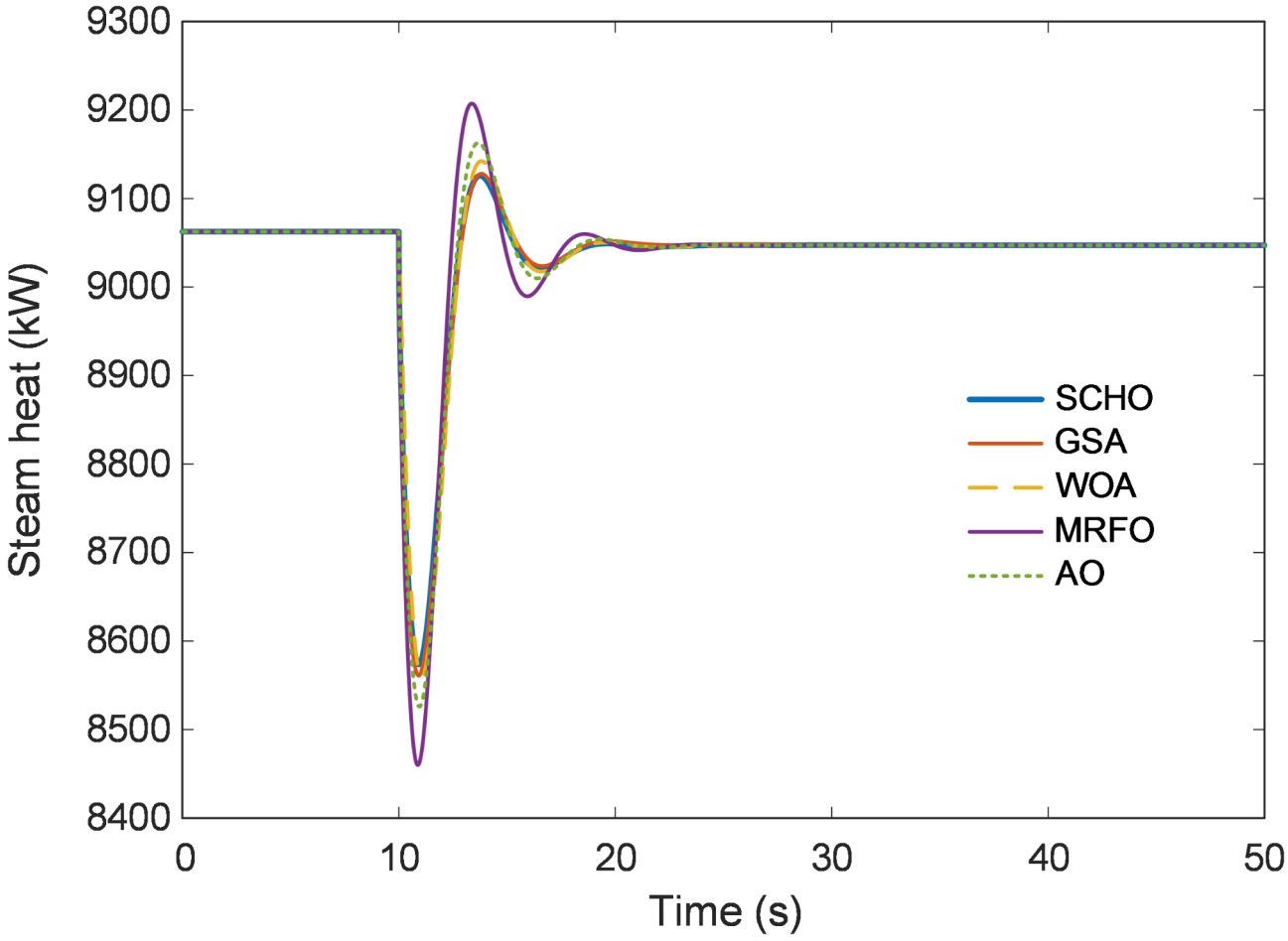


Fig. 16. Time response of steam heat.

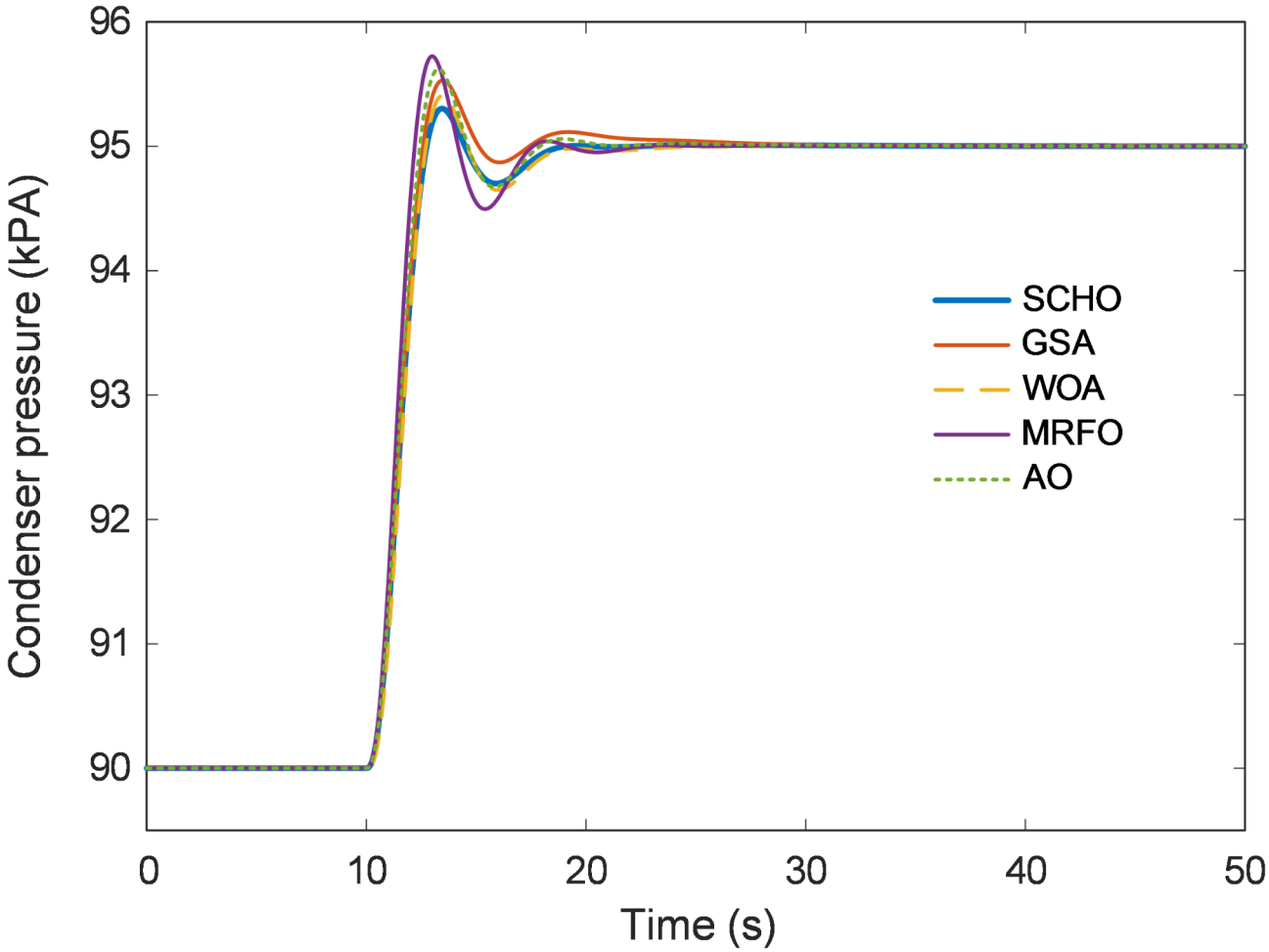


Fig. 17. Time response of condenser pressure.

Algorithms	ITAE	Normalized overshoot (%)	Normalized settling time (s)
SCHO	14.8078	6.0647	17.6635
GSA	19.5806	10.6107	20.0770
WOA	18.2824	8.1506	17.9283
MRFO	16.4532	14.4882	17.0708
AO	17.4650	12.4207	17.2855

Table 6. Numerical values of ITAE, normalized overshoot and settling time for various algorithms.

Data availability

The datasets used and/or analyzed during the current study available from the corresponding author on reasonable request.

Received: 30 July 2024; Accepted: 10 February 2025
Published online: 26 February 2025

References

1. Jan, A. Z., Kedzia, K., Abbass, M. J. & Fractional-Order, P. I. D. Controller (FOPID)-based iterative learning control for a nonlinear boiler system. *Energies (Basel)* **16**, 1045. https://doi.org/10.3390/en16031045 (2023).
2. Lachhab, N., Svaricek, F., Wobbe, F. & Rabba, H. Fractional order PID controller (FOPID)-toolbox. In *Proceedings of the 2013 European Control Conference (ECC)*. 3694–3699. (IEEE, 2013).
3. Izci, D., Ekinci, S. A. & Novel-enhanced metaheuristic algorithm for FOPID-controlled and Bode's Ideal transfer function–based Buck converter system. *Trans. Inst. Meas. Control* **45**, 1854–1872. https://doi.org/10.1177/01423312221140671 (2023).
4. Izci, D. & Ekinci, S. Comparative performance analysis of slime mould algorithm for efficient design of proportional–integral–derivative controller. *Electrica* **21**, 151–159. https://doi.org/10.5152/electrica.2021.20077 (2021).

5. Mohd Tumari, M. Z., Ahmad, M. A., Suid, M. H. & Hao, M. R. An improved marine predators algorithm-tuned fractional-order PID controller for automatic voltage regulator system. *Fractal Fract.* **7**, 561. https://doi.org/10.3390/fractalfract7070561 (2023).
6. Rashedi, E., Nezamabadi-pour, H. & Saryazdi, S. G. S. A. A gravitational search algorithm. *Inf. Sci. (N. Y.)* **179**, 2232–2248. https://doi.org/10.1016/j.ins.2009.03.004 (2009).
7. Mirjalili, S. & Lewis, A. The whale optimization algorithm. *Adv. Eng. Softw.* **95**, 51–67. https://doi.org/10.1016/j.advengsoft.2016.01.008 (2016).
8. Zhao, W., Zhang, Z. & Wang, L. Manta Ray foraging optimization: an effective bio-inspired optimizer for engineering applications. *Eng. Appl. Artif. Intell.* **87**, 103300. https://doi.org/10.1016/j.engappai.2019.103300 (2020).
9. Abualigah, L. et al. Aquila optimizer: a novel meta-heuristic optimization algorithm. *Comput. Ind. Eng.* **157**, 107250. https://doi.org/10.1016/j.cie.2021.107250 (2021).
10. Ekinci, S. et al. Frequency regulation of PV-reheat thermal power system via a novel hybrid educational competition optimizer with pattern search and cascaded PDN-PI controller. *Results Eng.* 102958. (2024).
11. Jabari, M. et al. Efficient DC motor speed control using a novel multi-stage FOPD(1 + PI) controller optimized by the Pelican optimization algorithm. *Sci. Rep.* **14**, 22442. https://doi.org/10.1038/s41598-024-73409-5 (2024).
12. Goud, B. et al. Power quality enhancement in PV integrated system using GSA-FOPID CC-VSI controller. *EAI Endorsed Scal. Inform. Syst.* **10**, 6 (2023).
13. Goud, B. et al. Dynamic voltage restorer to mitigate voltage sag/swell using black widow optimization technique with FOPID controller. *EAI Endorsed Trans. Energy Web* **10** (2023).
14. Kalyan, C. H. et al. Squirrel search algorithm based intelligent controller for interconnected power system. *Int. J. Model. Simul.* 1–21. (2023).
15. Gopi, P. et al. Performance and robustness analysis of V-Tiger PID controller for automatic voltage regulator. *Sci. Rep.* **14**, 7867. https://doi.org/10.1038/s41598-024-58481-1 (2024).
16. Naga Sai Kalyan, C. H., Sambasiva Rao, G., Bajaj, M. & Baseem Khan & Majeed Rashid Zaidan. Frequency regulation of geothermal power plant-integrated realistic power system with 3DOFPID controller. *Cogent Eng.* **11**, 1. https://doi.org/10.1080/23311916.2024.2322820 (2024).
17. Goud, B. S., Reddy, C. R., Bajaj, M., Elattar, E. E. & Kamel, S. Power quality improvement using distributed power flow controller with BWO-based FOPID controller. *Sustainability* **13**, 11194. https://doi.org/10.3390/su132011194 (2021).
18. Kalyan, C. N. S., Srikanth Goud, B., Reddy, C. R., Bajaj, M. & Srinivasa Rao, G. SMES and TCSC coordinated strategy for multi-area multi-source system with water cycle algorithm based 3DOF-PID controller. *Smart Sci.* https://doi.org/10.1080/23080477.2022.2054199 (2022).
19. Srikanth Goud, B. et al. AGC of multi area multi fuel system with water cycle algorithm based 3DOF-PID controller and integration of PEVs 2021 international conference on data analytics for business and industry (ICDABI), 464–469, https://doi.org/10.1109/ICDABI53623.2021.9655899 (2021).
20. Narasimha Prasad, T. et al. Salah Kamel, Power management in hybrid ANFIS PID based AC–DC microgrids with EHO based cost optimized droop control strategy. *Energy Rep.* **8**. https://doi.org/10.1016/j.egyr.2022.11.014 (2022).
21. Wang, J. S. & Li, S. X. PID Controller of steam condenser based on particle swarm optimization algorithm. *J. Comput. Theor. Nanosci.* **14**, 3698–3701. https://doi.org/10.1166/jctn.2017.6659 (2017).
22. Somasundar Reddy, C., Balaji, K. A. & Genetic algorithm GA)-PID controller for temperature control in shell and tube heat exchanger. *IOP Conf. Ser. Mater. Sci. Eng.* **925**, 012020. https://doi.org/10.1088/1757-899X/925/1/012020 (2020).
23. Olana, D. & Abose, F. A. Temperature controller design for shell and tube heat exchanger. *Int. J. Eng. Manuf.* **11**, 37–46. https://doi.org/10.5815/ijem.2021.01.05 (2021).
24. Suthar, H. A. & Gadit, J. J. Two degree of freedom controller optimization using GA for shell and tube heat exchanger. In *Proceedings of the 2017 11th International Conference on Intelligent Systems and Control (ISCO)*. 1–7. (IEEE, 2017).
25. Tugashova, L. G. & Zatonskiy, A. V. Comparison of methods for heat exchanger control. *Theor. Found. Chem. Eng.* **55**, 53–61. https://doi.org/10.1134/S0040579520060226 (2021).
26. Al-Dhaifallah, M. & Fuzzy Fractional-Order, P. I. D. Control for heat exchanger. *Alexandria Eng. J.* **63**, 11–16. https://doi.org/10.1016/j.aej.2022.07.066 (2023).
27. Oravec, J. et al. Robust model predictive control and PID control of shell-and-tube heat exchangers. *Energy* **159**, 1–10. https://doi.org/10.1016/j.energy.2018.06.106 (2018).
28. Girirajan, B., Rathikarani, D. & Optimal, C. R. O. N. E. Controller using meta-heuristic optimization algorithm for shell and tube heat exchanger. *IOP Conf. Ser. Mater. Sci. Eng.* **1166**, 012058. https://doi.org/10.1088/1757-899X/1166/1/012058 (2021).
29. Ahn, J. K. et al. PID control of a shell and tube heat exchanger system incorporating feedforward control and anti-windup techniques. *J. Inst. Control Rob. Syst.* **20**, 543–550. https://doi.org/10.5302/J.ICROS.2014.14.0009 (2014).
30. Alzakari, S. A., Izci, D., Ekinci, S., Alhussan, A. A. & Hashim, F. A. Nonlinear FOPID controller design for pressure regulation of steam condenser via improved metaheuristic algorithm. *PLoS ONE* **19**, e0309211. https://doi.org/10.1371/journal.pone.0309211 (2024).
31. Chen, C., Zhou, Z., Bollas, G. M. & Dynamic modeling simulation and optimization of a subcritical steam power plant. part I: Plant model and regulatory control. *Energy Convers. Manag.* **145**, 324–334. https://doi.org/10.1016/j.enconman.2017.04.078 (2017).
32. Maidi, A., Diaf, M., Corriou, J. P. & Optimal Linear, P. I. Fuzzy controller design of a heat exchanger. *Chem. Eng. Process.* **47**, 938–945. https://doi.org/10.1016/j.cep.2007.03.008 (2008).
33. Dugdale, D. Peng Wen Controller optimisation of a tube heat exchanger. In *Proceedings of the Proceedings of the 4th World Congress on Intelligent Control and Automation (Cat. No.02EX527)*. 54–58. (IEEE).
34. Wu, X., Shen, J., Li, Y. & Lee, K. Y. Steam power plant configuration, design, and control. *WIRE Energy Environ.* **4**, 537–563. https://doi.org/10.1002/wene.161 (2015).
35. Shin, D., Jeon, J., Kim, T., Park, J. H. & Kim, S. J. Development of the thermal performance model using temperature gradient analysis for optimized design of steam surface condenser. *Int. J. Heat. Mass. Transf.* **163**, 120411. https://doi.org/10.1016/j.ijheatmasstransfer.2020.120411 (2020).
36. Bai, J. et al. Abdel Wahab, M. A Sinh cosh optimizer. *Knowl. Based Syst.* **282**, 111081. https://doi.org/10.1016/j.knosys.2023.111081 (2023).
37. Shaukat, N. et al. International conference on energy and comparative study of control methods for steam condenser. In *Proceedings of the (ICECE)* 32–37. (IEEE, 2017).
38. Laskowski, R., Smyk, A., Rusowicz, A. & Grzebielec, A. A. Useful formulas to describe the performance of a steam condenser in off-design conditions. *Energy* **204** https://doi.org/10.1016/j.energy.2020.117910 (2020).
39. Li, S. X. & Wang, J. S. Dynamic modeling of steam condenser and design of PI controller based on grey wolf optimizer. *Math. Probl. Eng.* **2015**, 1–9. https://doi.org/10.1155/2015/120975 (2015).
40. Rao, C. S., Santosh, S., V, D. R. & Tuning Optimal, P. I. D. Controllers for open loop unstable first order plus time delay systems by minimizing ITAE criterion. *IFAC PapersOnLine* **53**, 123–128. https://doi.org/10.1016/j.ifacol.2020.06.021 (2020).
41. Mirzargar, M., Whitaker, R. T. & Kirby, R. M. Curve boxplot: generalization of Boxplot for ensembles of curves. *IEEE Trans. Vis. Comput. Graph* **20**, 2654–2663. https://doi.org/10.1109/TVCG.2014.2346455 (2014).
42. Hubert, M. & Vandervieren, E. An adjusted boxplot for Skewed distributions. *Comput. Stat. Data Anal.* **52**, 5186–5201. https://doi.org/10.1016/j.csda.2007.11.008 (2008).

43. Dao, P. B. On wilcoxon rank sum test for condition monitoring and fault detection of wind turbines. *Appl. Energy* **318** https://doi.org/10.1016/j.apenergy.2022.119209 (2022).
44. Xu, J., Tian, Y., Sun, Y. & Scutari, G. Distributed algorithms for composite optimization: Unified framework and convergence analysis. *IEEE Trans. Signal Process.* **69**, 3555–3570. https://doi.org/10.1109/TSP.2021.3086579 (2021).
45. Oliveira, G. N. S., Costa, T., Mohamed, M. A., Ilinca, A. & Marinho, M. H. N. Comprehensive case study on the technical feasibility of green hydrogen production from photovoltaic and battery energy storage systems. *Energy Sci. Eng.* https://doi.org/10.1002/ese3.1905 (2024).
46. Aljohani, T., Mohamed, M. A. & Mohammed, O. Tri-level hierarchical coordinated control of large-scale EVs charging based on multi-layer optimization framework. *Electr. Power Syst. Res.* **226**, 109923. https://doi.org/10.1016/j.epsr.2023.109923 (2024).
47. Liu, H. et al. An effective energy management layout-based reinforcement learning for household demand response in digital twin simulation. *Sol. Energy* **258**, 95–105. https://doi.org/10.1016/j.solener.2023.04.051 (2023).
48. Liu, Y., Yuan, D., Gong, Z., Jin, T. & Mohamed, M. A. Adaptive spectral trend based optimized EWT for monitoring the parameters of multiple power quality disturbances. *Int. J. Electr. Power Energy Syst.* **146**, 108797. https://doi.org/10.1016/j.ijepes.2022.108797 (2023).

Author contributions

Serdar Ekinci: Conceptualization, Methodology, Software, Visualization, Investigation, Writing- Original draft preparation. Veysel Gider, Davut Izci: Data curation, Validation, Supervision, Resources, Writing - Review & Editing. Laith Abualigah, Mohit Bajaj, Ievgen Zaitsev: Project administration, Supervision, Resources, Writing - Review & Editing.

Declarations

Competing interests

The authors declare no competing interests.

Additional information

Correspondence and requests for materials should be addressed to M.B. or I.Z.

Reprints and permissions information is available at www.nature.com/reprints.

Publisher's note Springer Nature remains neutral with regard to jurisdictional claims in published maps and institutional affiliations.

Open Access This article is licensed under a Creative Commons Attribution-NonCommercial-NoDerivatives 4.0 International License, which permits any non-commercial use, sharing, distribution and reproduction in any medium or format, as long as you give appropriate credit to the original author(s) and the source, provide a link to the Creative Commons licence, and indicate if you modified the licensed material. You do not have permission under this licence to share adapted material derived from this article or parts of it. The images or other third party material in this article are included in the article's Creative Commons licence, unless indicated otherwise in a credit line to the material. If material is not included in the article's Creative Commons licence and your intended use is not permitted by statutory regulation or exceeds the permitted use, you will need to obtain permission directly from the copyright holder. To view a copy of this licence, visit http://creativecommons.org/licenses/by-nc-nd/4.0/.

© The Author(s) 2025